VELOCITY STRUCTURE OF THE UPPER CRUST BENEATH THE EASTERN PLATEAU

By:

Tesfaye Hailu

APPROVED BY BOARD OF EXAMINERS:

Dr. Dereje Ayalew
Chairman
Signature

Dr. Tilahun Mammo
Advisor
Signature

Ato. Ketsela Tadesse
Examiner
Signature

Ato. Befekadu Oluma
Examiner
Signature

ACKNOWLEDGMENT

I am very grateful and indebted to my mentor and advisor Dr. Tilahun Mammo for his guidance through out the work. His complete confidence in me has given me the courage to finish this work from scratch. His expertise and solid criticism has helped me greatly in refining this work to the very last minute.

I also acknowledge the help I received from the staff of Yadot Business Group Plc, where people there give the utmost respect to education. Special thanks go to my superiors Ato Damtew Assefa and Ato Kebede Fekede of the Drilling Department, Ato Yoseph Tegegn and Ato Terefe Amberber, Managing director and System advisor to the company respectively. Yadot Business Group Plc. has supported me financially and logistically through out the work.

I have gleened much information from Dr. Dereje Ayalew from the Addis Ababa University, Department of Geology and Geophysics, Dr. Meseret Teklemariam from the Ethiopian Geological Survey and Ato. Negash Aweke from Saba Engineering Plc.

I would also like to thank Col. Teshome Abebe, Ato Sem Tekle, Ato. Djiregna Kenea, Col. Seyoum Abegaz and W/ro Fana Kebede who have been there all the way with me.

I owe Special thanks to all my friends for their much-needed assistance and their encouragement.

Finally, I would like to thank my family, my brothers Michael Hailu and Abel Hailu, my mother Felekech S/Mariam and my uncle Yimam Kebede. The unconditional love they gave me was the real esteem through the lapse of the work. They have supported me financially and morally. They have provided me the space and tranquility that I needed. I am greatly indebted and my deepest gratitude goes to you.

I dedicate this to my father, Hailu Kebede who is the one to inspire me. His life long encouragement to pursue my interest is the reason for all this work. Without him, none of this would have been accomplished.

TABLE OF CONTENT

LIST OF FIGURES AND TABLES

APPENDICES

ABSTRACT

Seismic and geologic sections are of vital importance to the various professional bodies, institutions and industries. They give us an insight on the grounds we are literally standing on. This study has conducted the subsurface imaging of the earth to a depth of 10 Km on a 98 Km long seismic profile line. The study was conducted starting from the foot of the eastern rift margin in to the eastern plateau to give us results, which are archetype to the study area.

For the generation of seismic waves explosives were detonated inside boreholes and programmable seismic energy recorders called "Texans" were deployed on the surface at about one kilometer spacing.

Reduced first arrival P – waves were picked and converted to actual time prior to inversion. The geoseismic model was inverted by the methods of the Generalized Reciprocal Method (GRM).

Four layers at an average depth of 2 Km, 5 Km and 7 Km were identified with corresponding average P-wave velocities of 2700 m/s, 4000 m/s, 5800 m/s and 6300 m/s respectively. The geological section of the studied area has been identified to rest on a crystalline basement overlain by low-grade metamorphic rocks. The first layer has been identified as the Oligocene – Miocene volcanics and the Mesozoic sediments.

A horst like structure has been identified at a locality known as Hamda – Diksis. The top part of the structure has a depth of 3.3 Km from the surface to its top and it is truncated sharply by the Assela-Sire border fault on the NW flank.

1. Introduction

The East African Rift System is one of the very few places in the world where active rifting processes can be observed. The way in which it is rifting is in accordance with the plate tectonic theory.

The geology and structures of the eastern plateau adjoining the rift system are partially controlled by the rifting process. The aim of this thesis is to map the P - wave velocity distribution of the layers in the upper most crust.

1.1 Previous works

Though deep seismic works were conducted in the nearby Afar Depression *(Berckhemer et al., 1975; Ruegg, 1975)*, no work has ever been done in the eastern plateau.

In regard to geology, however, some works have been reported *(Paul A. Mohr, 1962, 1963, 1966, 1967, 1970, 1971, Juch 1975, Baker et al., 1972, Rex et al., 1971, Jones & Rex, 1974, Kazmin V et al., 1974, 1976, V. Kazmin, May 1979, V. Kazmin AA, 1972, Kazmin & Berhe 1978, Di Paola, 1972, 1976, Zanettin et al., 1978, 1980)*.

1.2 Physiographic outlines

The region described in this study starts from the floor of the eastern rift margin and goes further south to a small town called Bele found in the Arsi administrative zone of the Oromia region.

The area of study is accessible by 4x4 vehicles through asphalt and gravel road. The study area starts at the floor of the eastern rift margin with an elevation of 1,300 mt a.s.l and quickly rises to an altitude of 2,500 mt a.s.l at the top of the eastern escarpment. It attains a local high of 2704 mt a.sl. on the plateau. This local highs and lows are found at a UTM Easting of 576799.3 and Northing 910661.2 and Easting of 564439.4 and Northing of 936347.4 Zone 37N respectively.

1.3 Aim of the present study

The major objectives of this work are:

1) Mapping the seismic layers beneath the eastern plateau along the EAGLE profile I.
2) Interpret the geology.
3) Identify structures if any.

1.4 Methodology

Refraction seismic method has been employed to produce the seismic model beneath the eastern plateau. The generalized reciprocal method (GRM) was used to analyze the data and invert the geoseismic model.

This seismic model was then interpreted in terms of geology using deterministic P-wave velocities, field investigations to correlate the results obtained in this work with that of the outcrops in the profile and previous regional geological works.

2. Regional Geology

The lithologic successions beneath the study area is underlain by an ancient Archaean Craton where the age is greater than 2500 m.y. In some parts of Africa, the pre-cambrian rocks, representing the first 5/6th of the solid earths history, can be separated into three great divisions, each newer one being less folded and metamorphosed than that which preceded it (Paul A. Mohr, 1971).

2.1 Paleozoic

The Paleozoic extends from the Cambrian to the Permian. During this period, the whole of the Arabo-Ethiopian massif formed a stable landmass subject to denudation resulting in near peneplanation of the ancient pre-cambrian orogenic mountain ranges at the end of the era. However, some doubtful local occurrences of the Paleozoic strata are worthy of note (Mohr 1971).

In the Paleozoic era, two lithological units are discernable; the edaga arbi glacials and the enticho sandstones. It has been noted that the unconformity between the Adigrat sandstone and underlying clastics is not significant. This shows that differentiation between the clastics of the Paleozoic and the Adigrat sandstones of the Mesozoic is barely possible.

2.2 The Mesozoic

Early in the Mesozoic the horn of Africa was marked by the first major transgression of the sea since the end of the pre-Cambrian. The epeirogenic sinking which carried this massive transgression over parts of the ancient continent of the Gondwana land commenced in Triassic. It reached its maximum development in the early upper Jurassic, after which regression due to eperogenic uplift followed By the end of the Mesozoic almost the entire horn of Africa was again raised above sea level (V.Kazmin A.A., 1972).

2.2.1 The Adigrat sandatone

This is a transgressive facies ranging from the upper Triassic age in the Ogaden to lower or possibly even middle Jurassic in Tigre and Eritrea. Induction therefore is that the sea advanced from the SE to the NW.

Whilst in a given part of Ethiopia the thickness of the Adigrat sandstone remains fairly constant. local variations are observed where irregularities in the basement complex peneplain occur. General figure of the central Ethiopia can be given as 500 mt, but variations in the thickness of the Adigrat sandstone are known as much as 1000mt and to as little as a few meters.

The Adigrat sandstone is generally massive and thick bedded. It generally comprises approximately 6/5 major lithologies where the thickness of one may range from maximum of 400 to less than 3 mt. In the Cherecher (Arussi) highlands the basal Adigrat sandstone formation underling the Jurassic limestone varies in thickness from 200mt in the Galleti valley in the SW to only 25 mt in the Ramis valley in the NE (V.Kazmin A.A., 1972).

2.2.2 The Antalo limestone facies

The Antalo limestone has been observed to be lying directly on the basement complex in northern or central Ethiopia, always being underlain by the Adigrat sandstone.

The Antalo limestone comprises many lithological types of limestone and includes layers of marl and silt. The Antalo limestone formation varies in thickness from 0 to 800 mt. In the Arussi highlands, the Mesozoic succession is up to 1000 mt.

In Chercher these occur 250 to 460 mt of limestone resting on the 150 mt thick Adigrat sandstone formation. However to the NE, this basal sandstone facies thins out until the limestone occurs resting directly on basement complex rocks (Mohr, 1971).

2.2.3 The regressive upper sandstone facies and rocks of cretaceous age

A new transgression began in the Aptian and this was also the time of a wide spread marine transgression in the whole Middle East. It is important that the first manifestation of basaltic volcanism coincides with the lower cretaceous transgression (tuffs and flows) in the Ambaradam formation – (Abate etal 1969).

In the Chercher highlands the upper sandstone occurred in irregularly distributed isolated outcrops. In the Soca valley 150 mt of upper sandstone is typically developed (Mohr 1971).

2.3 The Cenozoic

According to Zanettin & Justin – Visentin (1975) out crops of the Ashangi basalts (Eocene-Paleocene), are restricted to the north- central part of the Ethiopian plateau. Absolute age determination confirms the absence of pre-Oligocene basalts on the southeastern plateau. However Di Paola (1972) states that basalts and ignimbrites of the trap series (Eocene – late Miocene) occur on the top of the Ethiopian and the Somalian plateaux. Only in few places it is possible to observe unweathred basaltic lava flows of the trap series (quarries or highway trenches). This series is known to cover the Mesozoic marine sediments. The trap series is mostly made of basaltic lava flows with subordinately associated ignimbritic units intercalated between the basic lavas. According to .Mohr (1962, 1972) the trap series formed by fissure eruptions ages from Eocene-oligocene and is over lain by thick accumulations of the basaltic lavas erupted from the shield volcanoes on the Somali plateau. According to .Kazmin (1972), the name trap series usually applied to these rocks cover a considerable part of the Somalian plateau. This group is made of compact basalts. The thickest sections of this group occur close to the rift escarpment. (Mohr ,1967 a,b, 1971 c).

From late Miocene to Pliocene, volcanism was largely restricted to the rifts. But in some areas they cover the escarpments and even the adjacent plateaux (Kazmin 1972). According to Di Paola (1972) these are the last ignimbritic cover of the plateau.

3. Project EAGLE

3.1 Introduction

The Ethiopia Afar Geoscientific Lithospheric Experiment (EAGLE) is a major initiative to investigate how the African continent is splitting along the Ethiopian rift in the horn of Africa. The project involves the Universities of Leicester, Leeds, and Royal Holloway from the United Kingdom, Stanford University in California and the University of Texas at El Paso both from the United States. These groups are working with major groups from the Geophysical Observatory and the Department of Geology and Geophysics at the Addis Ababa University together with many scientists from the Ethiopian Geological Survey and the Petroleum Operations Department of the Ethiopian Ministry of Mines. The Commission of Science and Technology of the Democratic Federal Republic of Ethiopia coordinated the whole project.

The project included the carrying out of two seismic profiles; the first, profile 1, across the Ethiopian rift in the vicinity of Nazret extending to the Blue Nile in NW and to Ginir (in Bale region) in the south east; the second, profile 2, extended along the rift from Awassa in the south to Gewane in the north. A dense network of instruments (profile 3) was also to be deployed around the intersection of the two profiles to provide a 3-D tomographic image of the subsurface immediately beneath the neo-volcanic segment of Bosetti in the vicinity of Nazret (*Fig 3.1)*.

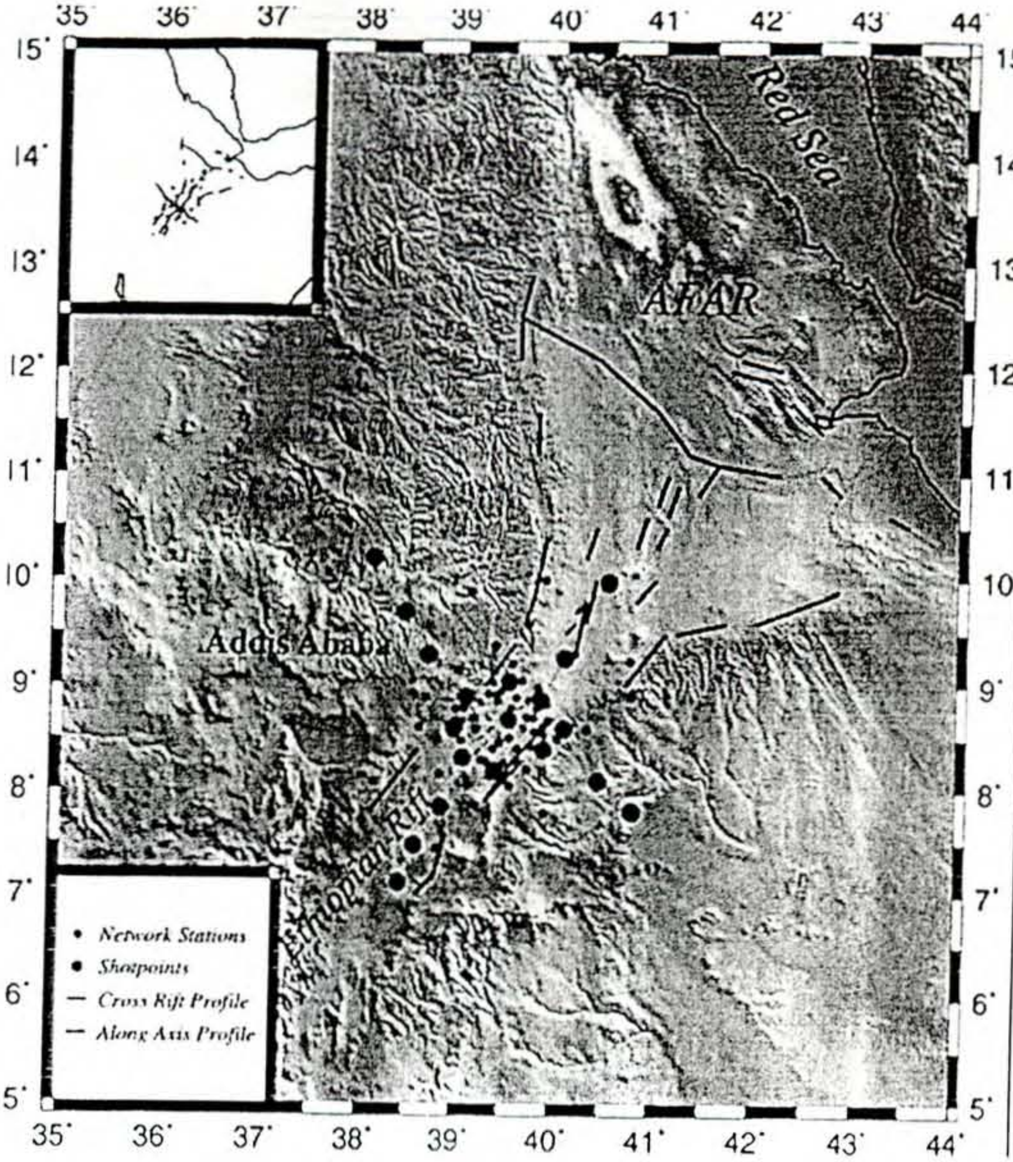

Fig 3.1Study Area showing profiles 1,2 and 3

The work was started in 2001 and finished by 2003. It involved recording of seismic "echoes" from the controlled explosions and natural earthquakes, to provide an image of the top 100 km or so of the earth over a region encompassing the northeastern part of the main Ethiopian rift where it enters afar. This project was divided into three phases where phase I involved 30 long term continuously recording seismic instruments being deployed over an approximately 250 x 250 km^2 centered on the volcanic segment in the rift valley immediately to the north-east of the town of Nazret. Phase II began in September 2002 and involved the deployment of a further 50 recorders within the phase I array, concentrating the density of recording the center of this region, in particular to study local earthquakes to refine our understanding of the patterns and origin of the local seismic activity.

3.2 The controlled source phase of the project

Phase III was the controlled source seismic study and was undertaken in January 2003. This project involved the deployment of nearly 1000 recorders over an 8-day period, which instruments will record the seismic waves generated from the detonation of 19 charges on both boreholes and lakes.

The instrumentation used in the project included two different types of seismic recorder; Guralp 6 TD broadband systems and Reftec Texan recorders.

The Guralp 6TDs come as a bundle with a 12V dry cell battery, solar panel, to energize these seismometers and a GPS clock receiver to synchronize their time round the clock. They were buried level and oriented north in a hole approximately 50 – 75 cm depth. They were deployed at a nominal spacing of 4 -- 5 km.

Both the Guralp 6TDs and the Reftec Texans were deployed using a deployment sheet. This sheet not only helped in the easy recovering of the seismometers but also to identify the location of each seismometer for the understanding of the data it has recorded.

4. Basics of the methods used in this work

4.1 Seismic Waves

Controlled source seismology involves the detonation of seismic explosive charges in deep boreholes distributed along a profile of seismic recording instruments deployed at regular intervals along the surface. The seismic waves generated by the charges travel down into the crust of the earth and are reflected and refracted back to the surface from geological interfaces in the earth. The seismic instruments record the resulting seismic waves as they reach the surface of the earth along the profile.

Of the many seismic waves generated during the explosion, only the refracted waves will be treated in this work.

4.2 Behavior of refracted waves from shot to recorder.

Seismic elastic wave is a form of energy, which travels through a medium depending on its elastic property. It is by vibrating the particles of the medium that seismic waves travel inside the earth. Energy could be released from a controlled source which could be a mere smite of the surface by a hammer or through the detonation of explosives inside a borehole as treated in this work. On the other hand, the energy could also be natural such as earthquakes. The way in which this energy is disseminated is in the form of seismic waves emanating from the source traveling outward in a spherical way in two main types of waves; body waves and surface waves.

The former are further subdivided into two namely P and S waves while the latter are divided into Raleigh and Love waves.

P waves also known as primary/ compressional / longitudinal waves; travel by vibrating the rock particles in the direction of their propagation. Their names are typical of their behavior for the particles are vibrated in a continuous rarefaction and compression.

Of all the waves that are generated during an explosion, P waves as their name implies are the first ones to arrive on the seismograph. But when doing so they follow three natural rules while traversing inside the earth.

Primarily, they follow Fermat's principle, which states, "Seismic waves travel in paths requiring the least time". The seismic waves after being generated are refracted when they intercept a media of different acoustic property (*Fig. 4.1*). Snell's law states, "The directions of the reflected and refracted waves traveling away from a boundary depend on the direction of the incident wave and the speeds of the waves".

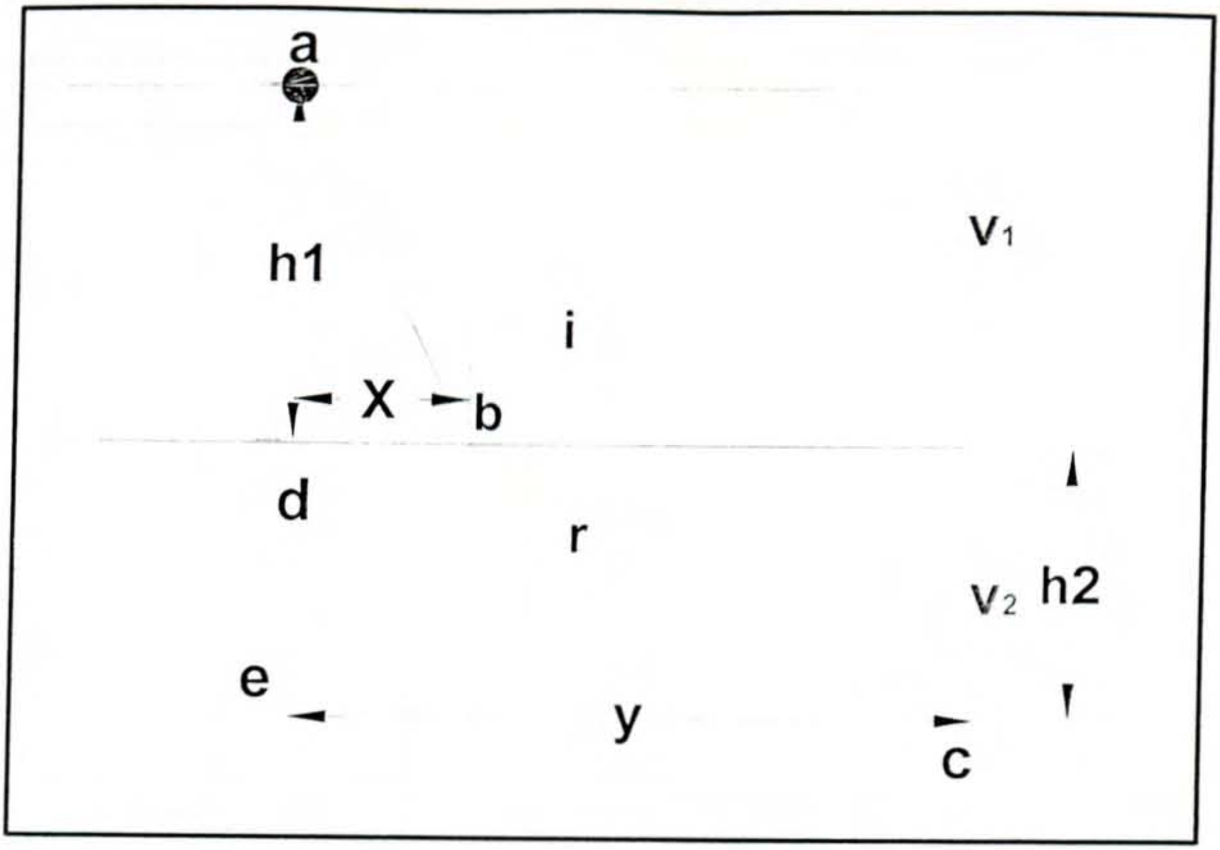

Fig 4.1 Diagram showing how seismic waves refract at an interface

$$\frac{v_1}{v_2} = \frac{\sin i}{\sin r} \qquad \textit{Eqn 4.1}$$

Equation 4.1 is also known as the Snell's law. For an elastic wave to propagate from one point to another through a path taking the least time should follow Snell's law.

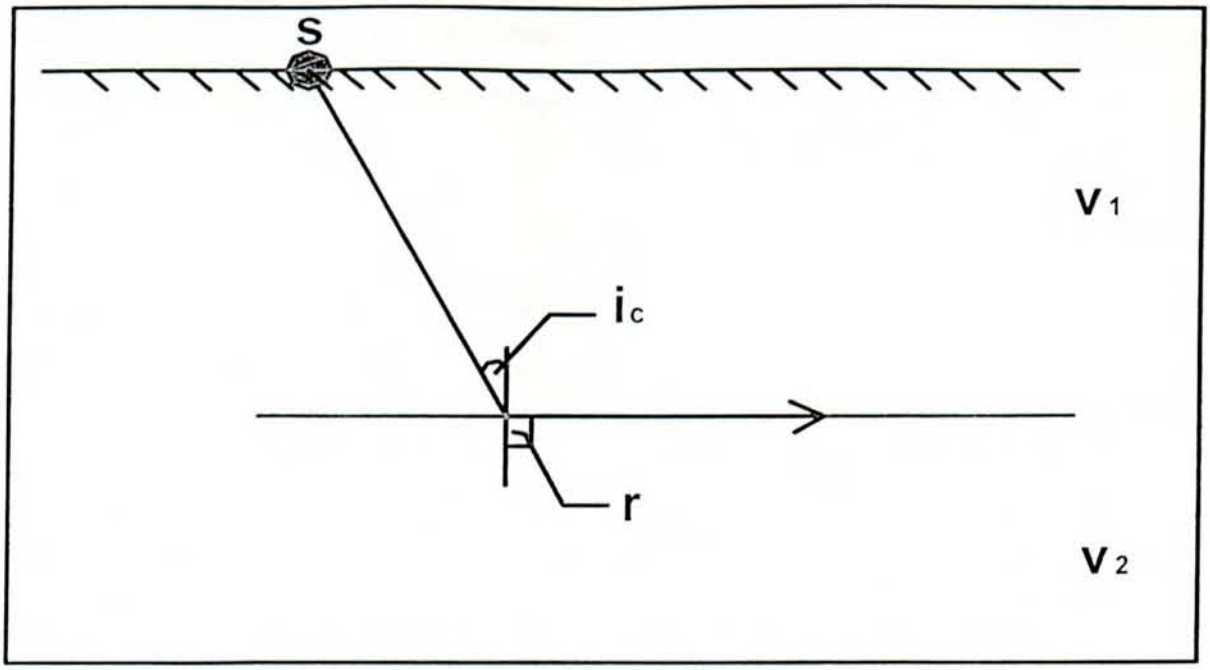

Fig 4.2 Diagram showing the critically refracted wave

Figure 4.2 shows that at critical angle of incidence, the wave is refracted in a horizontal direction or is "critically refracted" as Snell puts it. For this particular case, the angle of refraction = 90^0 and snell's law becomes

$$\sin i_c = \frac{v_1}{v_2} \qquad \textit{Eqn 4.2}$$

It is worth noting from equation 4.1 the following three points,

a) If $v_1 = v_2 \rightarrow i = r$, then there is no refraction

b) If $v_1 > v_2 \rightarrow i > r$, then there is no way we can record the refracted waves.

c) If $v_1 < v_2 \rightarrow i < r$, then the refracted waves go up to the surface.

This critically refracted wave is made of infinite amount of point explosions, which simulate infinite amount of explosions inside the earth. Hence energy from within the earth is again released and reaches the surface to be recorded. This principle is known as Huygen's principle.

After the seismic energy has been critically refracted and started to rise up according to Huygen's principle, then again, it is the ray with an angle equal to the critical angle of incidence that reaches the surface first. Mathematically, it is shown below.

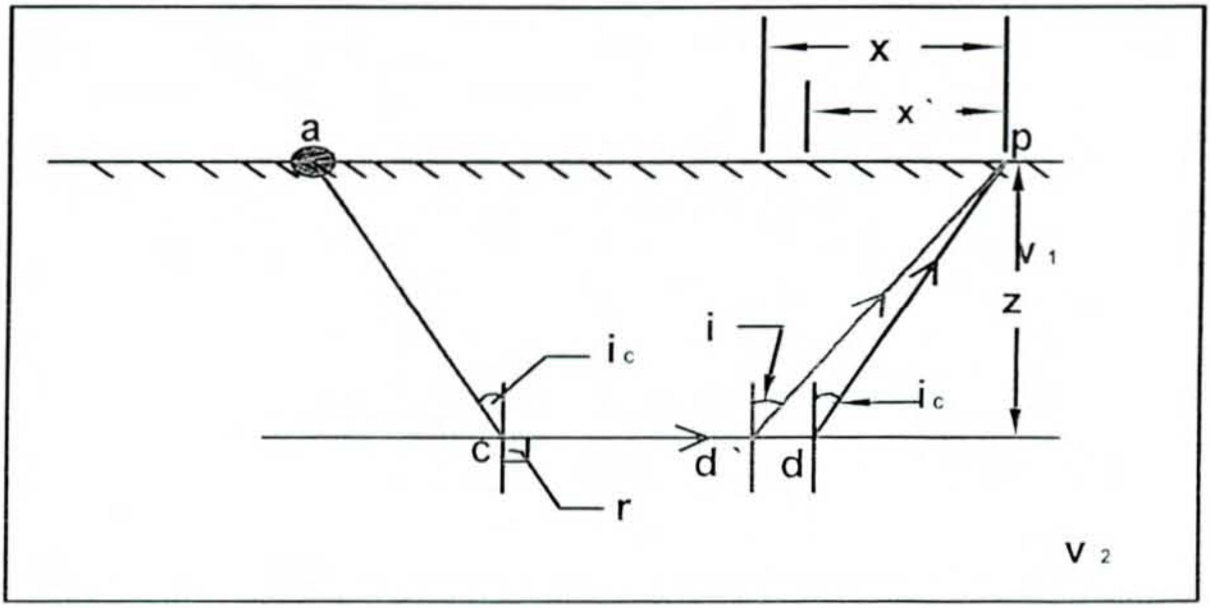

Fig 4.3 Diagram showing two different waves emerging from the 2^{nd} layer at different angles of refraction

Path I – acdp – t_1

Path II – acd`p – t_2

$$t_1 = \frac{ac}{v_1} + \frac{cd}{v_2} + \frac{dp}{v_1}$$

$$t_2 = \frac{ac}{v_1} + \frac{cd`}{v_2} + \frac{d`p}{v_2}$$

$$t_1 - t_2 = \frac{z}{v_1 \cos i`}\left[\cos(i_c - i) - 1\right] \qquad \textit{Eqn 4.3}$$

As $t_1 < t_2$ the path followed by the wave, according to Fermat's principle will be Path I. And hence the seismic wave that arrives first on the surface is the refracted wave, which has the same angle as the critical angle of incidence.

4.3 Generalized Reciprocal Method (GRM)

This method was first developed and later introduced by the Australian scientist Derecke Palmer at the 50th annual international SEG meeting in November 18, 1980, Houston. The GRM is a technique for delineating undulating refractors at any depth from inline seismic refraction data consisting of forward and reverse travel times.

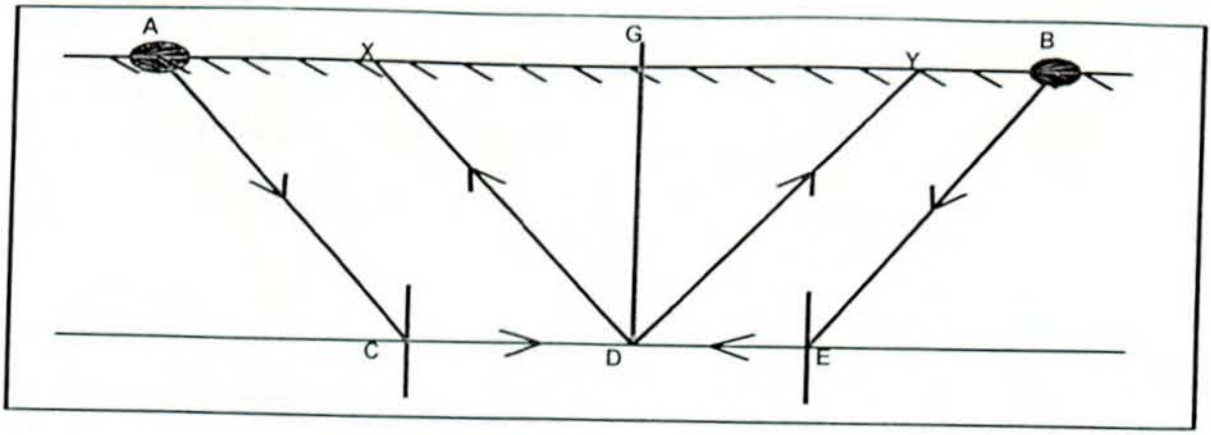

Fig 4.4 Diagram showing the forward and reverse shots with the variable distance XY

The traveltimes at two geophones, separated by a variable distance XY (*Fig 4.4)*, are used in refractor velocity analysis and time depth calculations. At the optimum XY spacing, the upward traveling segments of the ray to each geophone emerge from near the same point on the refractor. This results in the refractor velocity analysis function being the simplest and the time-depth being the most detail.

The GRM provides a means of recognizing and accommodating undetected layers provided an optimum XY value can be recovered from the travel-time data, the refractor velocity analysis, and or the time depth. The presence of undetected layers can be inferred when the observed optimum XY value differs from the XY value calculated from the computed depth section. The undetected layers can be accommodated by using an average velocity based on the optimum XY value. This average velocity permits accurate depth calculations with commonly encountered velocity contrasts (D. Palmer 1980).

4.3.1 Optimum XY value

The optimum XY value is obtained based on the velocity analysis function t_v (*Eqn 4.4)* being the smoothest and the time depth function (*Eqn 4.5)* being the most detailed.

t_v = *velocity analysis function*

t_{AY} = *forward time from shot A to the geophone at Y*

t_{BX} = *Reverse time from shot B to the geophone at X*

$$t_v = \frac{t_{AY} - t_{BX} + t_{AB}}{2} \qquad \textit{Eqn 4.4}$$

The shot geophone positions are shown in figure 4.4. The plot of the velocity analysis curve verses offset would be smooth because at the optimum XY value, the seismic wave refracts from nearly the same point.

t_g = *time depth function*

v'_n = *Apparent velocity determined from the velocity function*

$$t_g = \frac{1}{2}\left[t_{AY} + t_{BX} - \left(t_{AB} + \frac{XY}{v'_n}\right)\right] \qquad \textit{Eqn 4.5}$$

By time depth function, it can be defined as the measure of depth to the refractor in units of time. This function is converted as depth in units of space using equation 4.6

$$t_g = \sum_{j=1}^{n-1} Z_{jg} \frac{\left(v^2{}_n - v^2{}_j\right)^{1/2}}{v_j v_n} \qquad \textit{Eqn 4.6}$$

Where Z_j gives us the layer number. Note that t_g is measure of depth in units of time and Z_g is measure of depth in units of space. Hence,

$Z_g = t_g \, . \, DCF$

DCF = depth conversion factor.

The optimum XY value we obtained using the above two functions is known as the observed XY value. XY value is then calculated using the apparent velocity obtained from the velocity function using the equation 4.7

$$XY = 2\sum_{j=1}^{n-1} Z_{jg} . \tan i_{jn} , \qquad \textit{Eqn. 4.7}$$

Where $i_{jn} = \sin^{-1}\left(\frac{v_j}{v_n}\right)$

The X Y value we observe and calculate should be the same to an acceptable limit. If not then it implies that there is a hidden layer present.

If $XY_{calc} = XY_{obs}$ *(No hidden layer)*

If $XY_{calc} > XY_{obs}$ *(Velocity inversion)*

If $XY_{calc} < XY_{obs}$ *(Thin layer)*

Hence once a hidden layer is observed, then the average velocity is used to map the hidden layer. This average velocity is defined in equation 4.8 below;

$\bar{v}$ = *Average velocity*

$$\bar{v} = \left[\frac{v'^2_n XY}{XY + 2t_g v'_n} \right]^{\frac{1}{2}} \qquad \text{Eqn 4.8}$$

and depth to the refractor is defined in Equation 4.9,

Z_{ref} = *Depth to the refractor*

$$Z_{ref} = \frac{t_{GV}}{\cos i}, i = \sin\left(\frac{\bar{v}}{v'}\right) \qquad \text{Eqn 4.9}$$

5. Data Acquisition

5.1 Borehole drillings

Saba Engineering Plc. was given the contract to drill six scientific wells in July 2002. The holes were drilled to be 10" in diameter and 50 mt deep, though this configuration was not kept at some drill sites. The drilling was conducted by the use of rotary rigs where all the wells were drilled through the use of DTH (*Robinson, 1992)* methods. At sites where more than one hole was drilled, the distance was kept at a minimum of 45 mt so that the explosion from one would not detonate the charge in the other hole. Two holes were drilled at sites where they were needed to produce a higher energy from the detonation. Drilling of the wells was finished by January 2003.

The holes drilled were far away from tukuls, cottages, buildings, bridges, underground pipelines, electric mains, etc. This was to ensure the safety of the communities and their infra structure. The location of the shot holes after optimizing safety and higher s/n ratio is shown in Table 5.1.

Shot point	Name	Easting	Northing	Zone	Elevation
14	Chefe Donsa	513316.39	992624.9	37N	2369.5
15	Doni A	562852.55	942514.5	37N	1226
25	Doni B	568062.56	943140.5	37N	1236
16	Kula	575890.59	886436.8	37N	2497.6
17	Bele	613879.67	854243	37N	2417.6
18a	Delo Sebro	667362.99	799874.1	37N	2159.2
18b	Delo Sebro	667248.67	799777.6	37N	2156.6

Table 5.1 Shot points with their position and elevation

The drilling of these holes was successfully finished except for SP 14, where there was blockage inside the hole, which disallowed the full unloading of the explosive.

The drilling log for SP 15, 25, 16, and 17 *(Appendix 3)* describes the physical nature of the boreholes. The full report on the geological log can be obtained form the drilling company Saba Engineering Plc., Addis Ababa, Ethiopia

5.2 Shooting and Texan deployment phase

5.2.1 Seismic sources

Sources of seismic energy come in a variety of sizes and shapes. Anything that causes motion on the ground could be defined as source of seismic energy. The type of seismic energy source used for this particular work is an explosive. The pros and cons when using this source were considered and are described below.

Advantages: -

- ✓ These t ypes o f s ources i mpound t he h ighest a mount o f s eismic energy, which are a direct function of the type and size of the explosives used.
- ✓ The energy tends to be of very high frequency
- ✓ These types of sources are usually placed inside a borehole, which tends to reduce the generation of surface waves
- ✓ Explosive sources are repeatable.

Disadvantages: -

- ✓ Safety
- ✓ Obtaining permission to using these sources is difficult.
- ✓ Data acquisition using this sources is much slower than using other sources. This is primarily because boreholes must be drilled within which explosives are to be placed
- ✓ Explosives tend to be expensive to acquire and maintain.

5.2.2 Shot details

The whole procedure of transporting the explosives, unloading them at their respective sites, shooting them and returning to Addis Ababa lasted from January 9 to the 15th 2003. The shots were conducted between January 11 and 13 *(Table 5.3)*. The explosives and their accessories that were transported to the site include;

a) 8.4 ton power gel C+ *(Fig 5.1)*, where the main explosive is packed in 25 Kg boxes each containing two 12.5 Kg packages of diameter 210mm and length 300mm.

b) Multi prime boosters, each 0.5 Kg to detonate the power gel.

c) Cordtex *(Fig 5.2)* detonating or primacord, to connect the boosters.

d) Electric seismic detonators *(Fig 5.3)* to initiate the explosives.

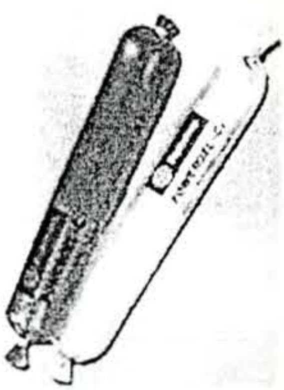

Fig 5.1 Power gel C+

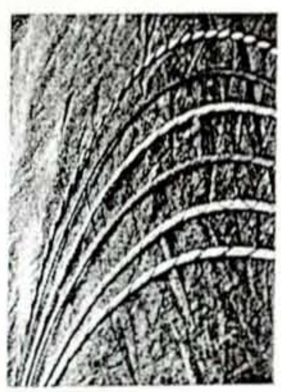

Fig 5.2 Cordtex Wires

Fig 5.3 Seismic detonators

The power gel C+ *(Fig 5.1)* explosives were buried to 30 mt of the surface *(Table 5.2)*. The boosters were positioned at regular intervals along the length of the hole. The primacords were connected along the whole length of the hole where their ends were tightly tapped together to the detonator.

The top part of the hole was stemmed according to the EAGLE specification. The specification was two parts of 15mm angular chippings to one part of wet sand to provide containment and to prevent blowout. The holes were stemmed with 3 Cu m of stemming. The stemming was needed in part to

a) Contain the explosion into the ground so that there would not be any damages caused to humans or property.

b) If the explosion is contained in the ground, it also gives higher energy, which is directly related to more energetic shock waves.

Shot point	**Name**	**Target Gel to be loaded**	**Actual Gel weight loaded**	**% Of actual target loaded into the borehole.**	**Comments**
14	Chefe Donsa	1000	375	37.50	Short loaded due to blockage of hole
15	Doni A	1000	50	5.00	Short loaded due to safety reasons
25	Doni B	1500	1025	68.33	Short loaded due to safety reasons
16	Kula	1000	1100	110.00	Over loaded from the extra gel obtained from the short loaded holes due to different reasons.
17	Bele	2000	2500	125.00	Over loaded from the extra gel obtained from the short loaded holes due to different reasons.
18	Delo Sebro	2000	2200	110.00	Over loaded from the extra gel obtained from the short loaded holes due to different reasons.

Table 5.2 Shot points and amount of charge loaded

The time of blast for each shot *(Table 5.3)* was precisely set on the shooting boxes, which had satellite (GPS/Leicester, El-Paso or USGS) timers where they are synchronized with the recording Texans. All the charges were detonated after 12.00 mid night local time, times where S/N was considered to be high.

Shot point	**Name**	**Shot date**	**Shot time GMT**	**Timer**
14	Chefe Donsa	Jan-12-03	21:03:00	GPS/Leics
15	Doni A	Jan-12-03	22:50:00	El Paso
25	Doni B	Jan-12-03	21:50:00	El Paso
16	Kula	Jan-13-03	21:10:00	USGS
17	Bele	Jan-12-03	21:10:00	USGS
18	Delo Sebro	Jan-11-03	21:29:56	USGS

Table 5.3 Shot point, time of shot and Timer

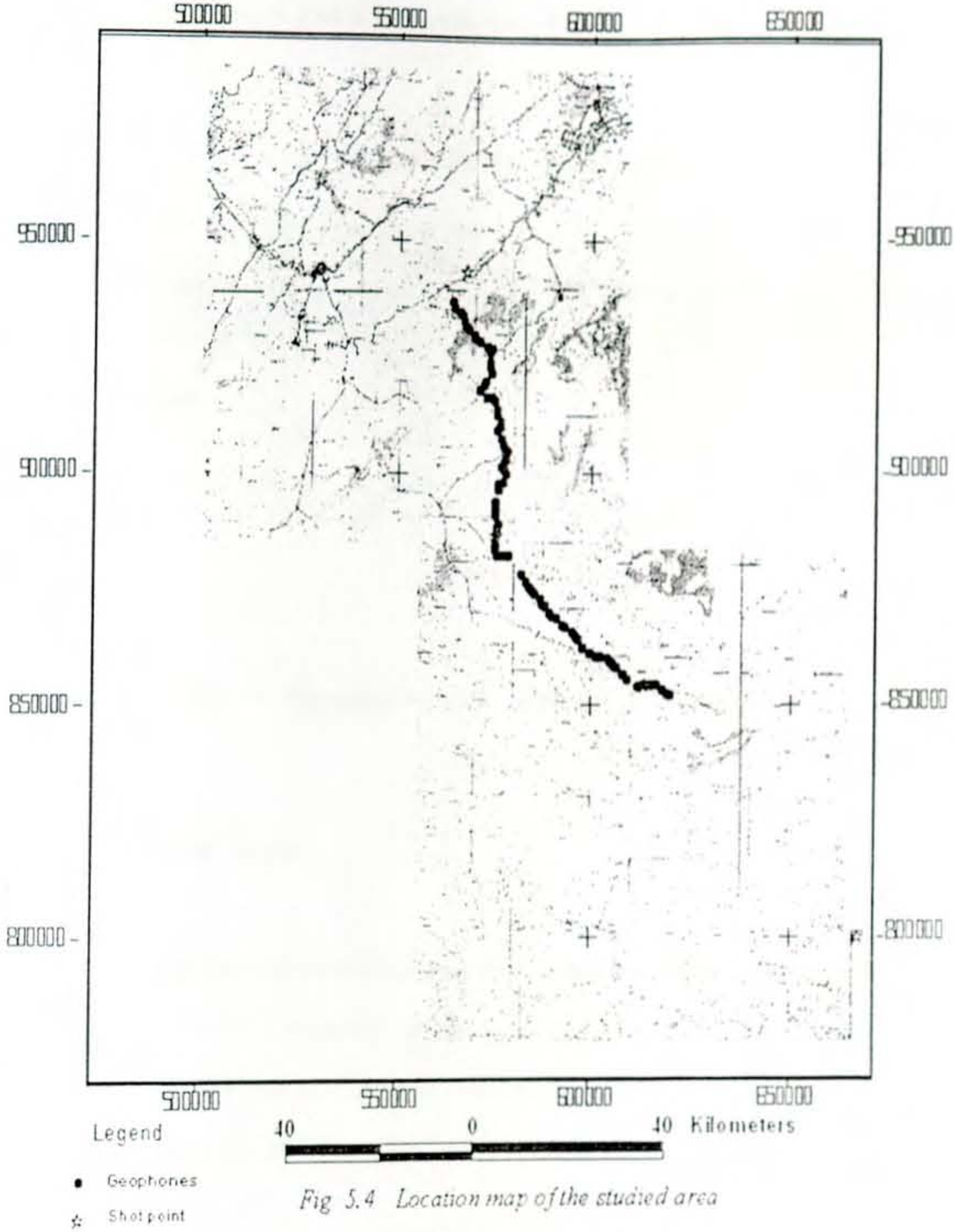

Fig 5.4 Location map of the studied area

Generally the altitude of the study area increases when climbing the eastern escarpment and attains a more or less constant value of 2500 m a.s.l. on the eastern plateau *(Fig 6.9)*.

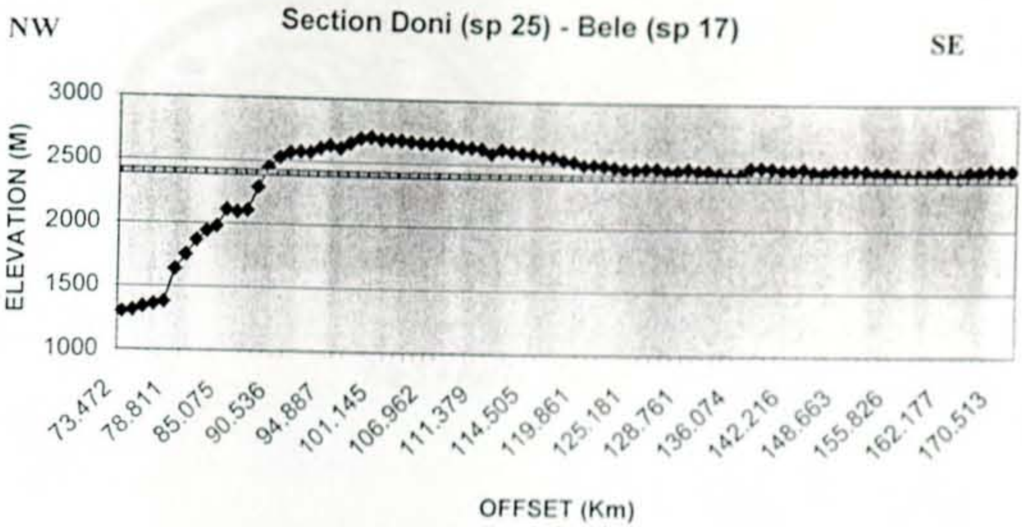

Fig 5.5 Diagram showing the section of the study area

5.2.3 Ref Tec 125-01 "Texan"

The name Texan *(Fig 5.6)* is given to a miniature seismic recorder, which is produced from a joint project among the Texas Universities seismic instrumentation alliance (which includes the Universities of Texas at El Paso, Rice University and the University of Texas at Dallas). The Texan is the present day leading edge technology seismic wave recorder.

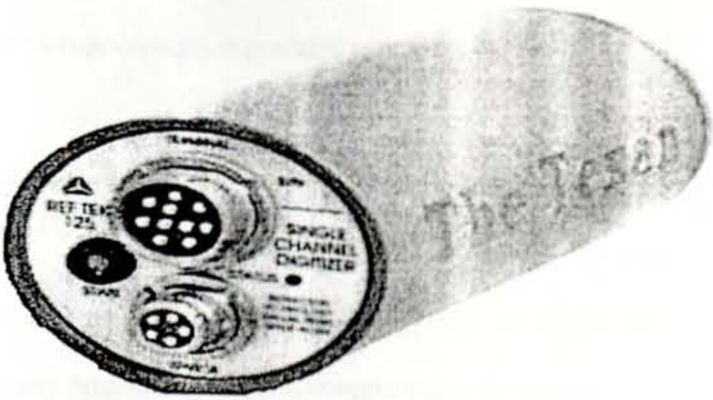

Fig 5.6 RefTec Texan

The particular model used in this project is the Ref-Tec 125-01 "Texan". These instruments have been supplied by the University of Copenhagen and IRIS / PASSCAL - University of Texas at El Paso.

5.2.3.1 Features of the Texan

These instruments could be used for

a) Active source crustal studies Refraction

b) Active source crustal studies Reflection

Their features are described briefly below

a) Powered from two 'D' cell batteries.

b) GPS synchronization

c) Recordings are made based on pre set time windows at a rate of 100 samples per second (SPS).

d) Timing accuracies for the recording period must be within +/- 5 msec relative to the shot time.

e) 32MB data Storage capacity expandable to 64MB.

5.2.3.2 Instrument operation

Texans feature a low noise differential input amplifier, 24-bit analogue to digital converter. The transit case has many functions in addition to containing, storing and transporting the geophones. This transit case includes interconnection cables (125 bus), which helps to easily connect to the external control device also known as the Bridge.

Functions of the bridge include

a) Transmit data between the 125 bus and the TCP/IP Ethernet bus, which enables the user interface program (UIP) to run on either a windows or Unix work station.

b) Routes the 111A GPS receiver/clock signals to each Texan for synchronizing internal time to UTC.

c) Supplies power to the Texans for setup and data retrieval.

After setup, the Texans are deployed for recording. A state LED displays the operation condition of the Texan. Green light indicating that

a) Battery voltage is sufficient

b) Acquisition program loaded

c) The unit is either ready to acquire data or is doing so.

Red light signifying that one or the whole above functions is not set

5.2.4 Recording instruments deployment phase

Since the operation of these Texans is dependent on the alkaline batteries, they were programmed to operate to the maximum time available. They were programmed for a one-hour window for each shot and then to stop. The way they were programmed was to start recording within the window where when the shots were fired. All the Texans had the same information on when to start and to stop. Their internal clock was synchronized to a clock that generates timing pulses using GPS signals.

At an instant, any amount of Texans could be programmed by attaching them together through the bridge and when the programming is done, they are made to switch to their internal batteries and ready to be deployed. They are designed to be a single channel recorder with a 4.5 Hz geophone attached to them. Their battery life lasted for eight days where they were deployed for two days, recorded for four days and finally recovered within two days before their battery life is dead.

The deployment was done between January 10 & 11, in the year 2003. When deploying these Texans, the following package went as a bundle;

- ✓ Road Logs - containing directions, distances and contact details for each site
- ✓ Maps - 1:250K and 1:50K maps with sites and routes marked.
- ✓ Relevant Permission Letters for the deployment region
- ✓ GPS with deployment sites way marked where needed
- ✓ Instrument Deployment and Recovery sheets
- ✓ Letter explaining the project in Amharic, Oromifa and English to be buried with the Texan and handed to any locals.

During deployment, it was done in a manner that they could be easily recovered and yet the site should be one with minimum noise and maximum security. Almost all of the Texans were deployed along side the off road. This was deemed appropriate for easy retrieval.

They were buried in approximately 0.15 mt depths with the geophone being inserted into the ground with a maximum vertical alignment *(Fig 5.7)*.

Fig 5.7 Texan buried inside the ground

Easting, Northing and elevation data was taken for each geophone *(Appendix 1)*. In addition to this, the station number, the unit serial number, comments, which help in the easy retrieval of these instruments, were noted on a sheet. These Texans were deployed in an approximate distance of one kilometer and deployment jumped at sites where the Guralp 6-TD *(Sec 3.2)* seismometers were present. For detailed Texan-shot, Texan-Texan distance *(Appendix 2)*.

At the conclusion of the experiment, the Texans are returned to the setup facility, retrieved and the data downloaded to the workstation for processing. The early retrieval phase of these instruments was of crucial importance. This is because, their battery had lifetime of eight days. After being synched to a GPS clock, these Texans keep track of time using their internal batteries. Though the data is registered with time, it is not the actual time that is registered rather relative.

After being retrieved, the Texans are switched to an external power and the raw SEG-Y data is backed up and later uploaded to a server. When being switched to the external batteries, it is important that the internal batteries are running. If not then there would not be the stop information and the data from the last shot would be useless for that particular Texan.

6. Data processing

The data processing includes

a) Picking of first arrivals.

b) Converting these first arrivals values from their reduced arrival time to their actual arrival time.

c) Feeding the arrival times, to the inverting software including information on offset distances and elevations.

d) Assigning layers on the travel time curves.

e) Inversion of the assigned layers to produce the geoseismic model.

6.1 Reduced arrival times

The raw data was reduced by assuming average crustal velocity of 6000 m/s. The distance of each geophone from the shot was known; hence the traces were reduced in time with the basic formula

$$t = \frac{X}{V_c} \qquad \textit{(Eqn 6.1)}$$

X = distance of the geophone to the shot.

V_c = Crustal velocity = 6000 m/s

This reduction was imperative because the scale of the experiment was very huge and the attempt to view all the seismic traces would be ludicrous for reasons of scale. Figures 6.1 – 6.6 show reduced arrival times for each geophone from each shot. The picked reduced first arrival time of each geophone lie within the window of 0 – 2 sec (*Fig 6.1 – 6.6, Appendix 4*).

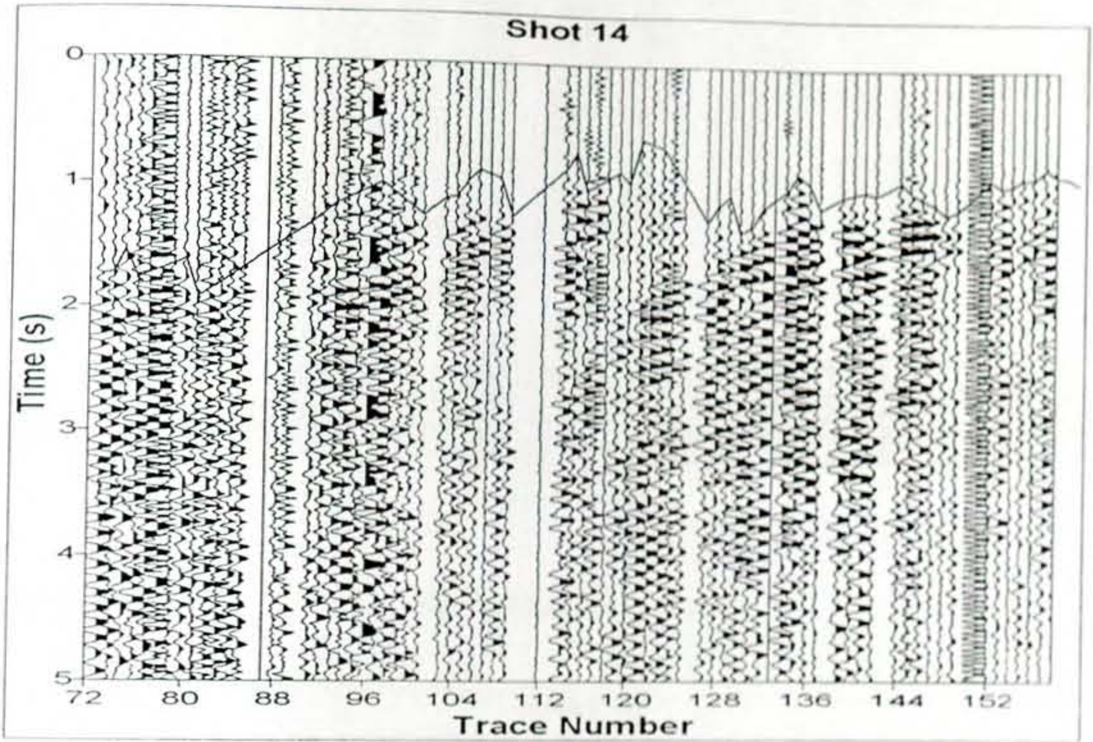

Fig 6.1 Traces from shot 14

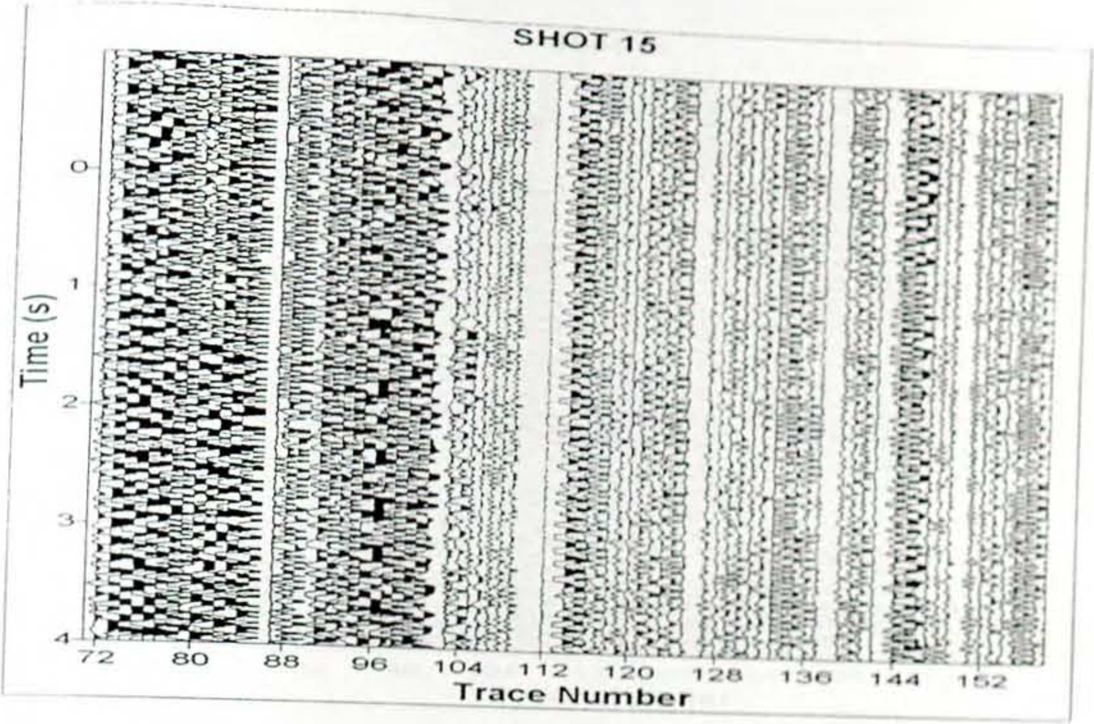

Fig 6.2 Traces from shot 15

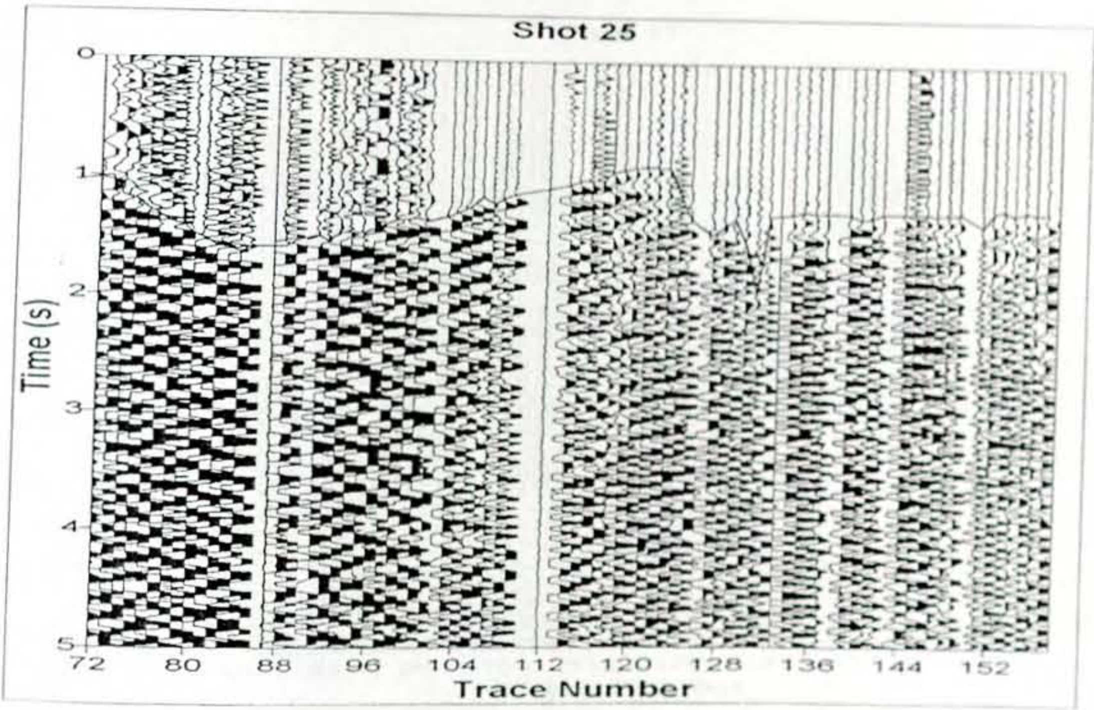

Fig 6.3 Traces from shot 25

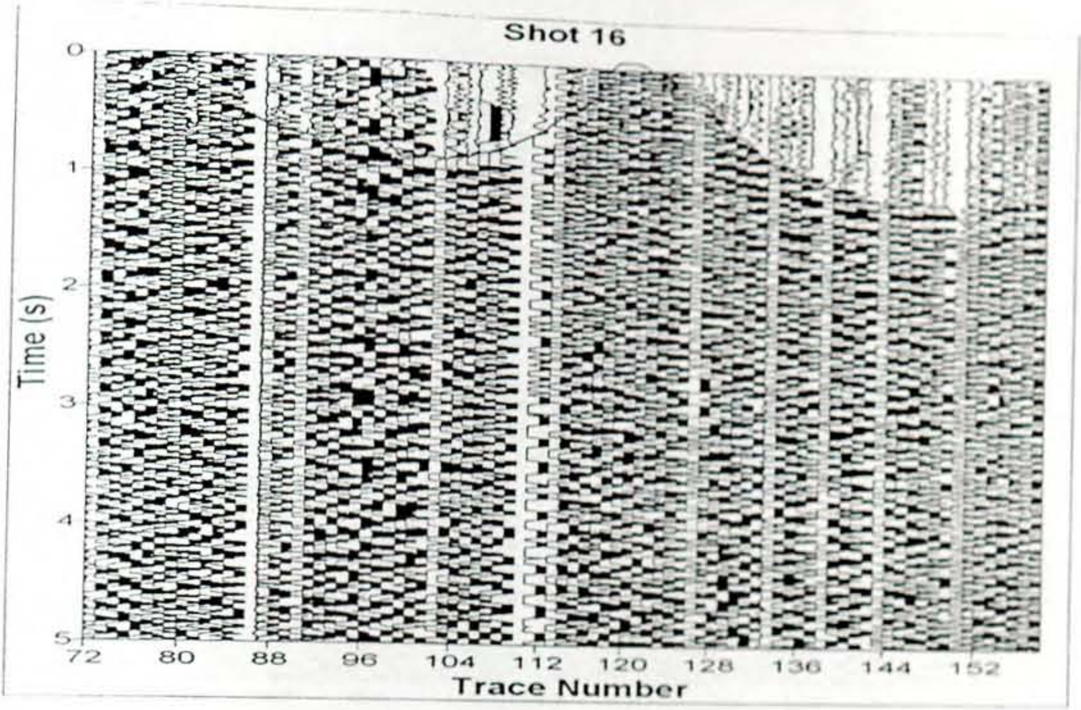

Fig 6.4 Traces from shot 16

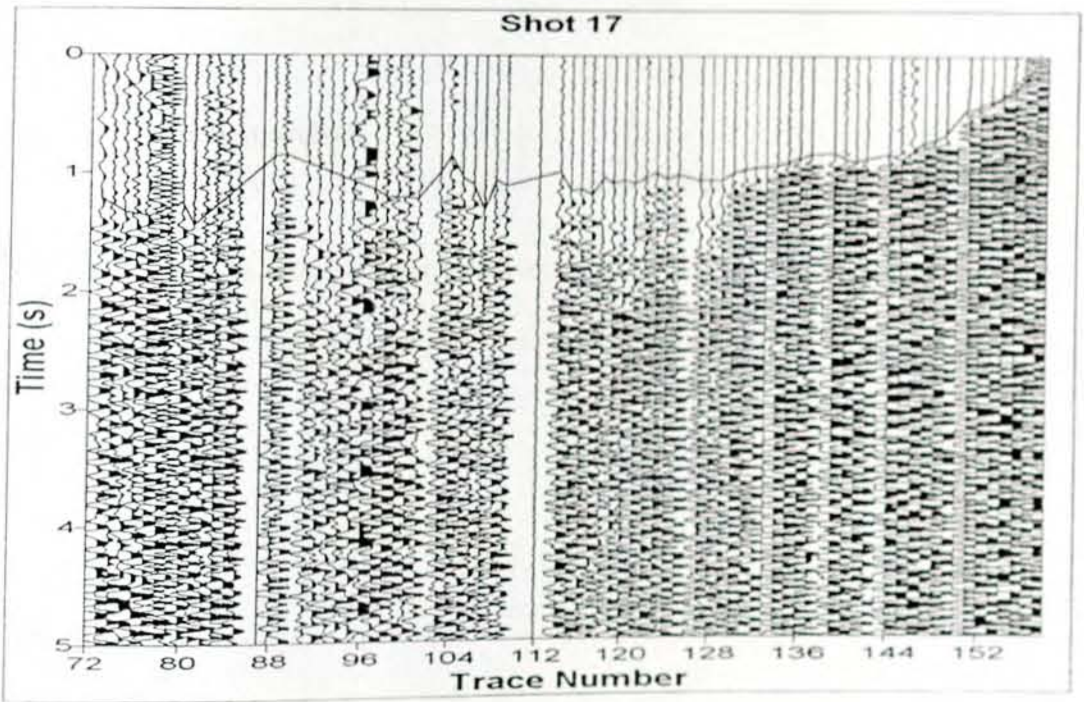

Fig 6.5 Traces from shot 17

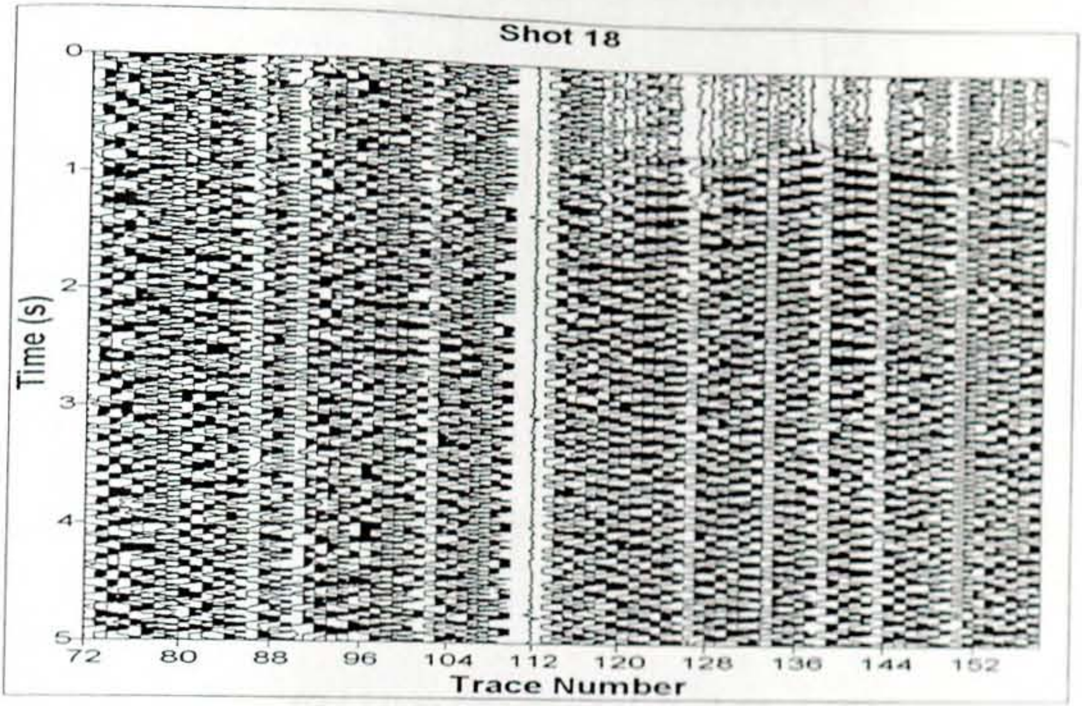

Fig 6.6 Traces from shot 18

6.2 Picking of the first arrivals

The first arrivals are the refracted Crustal p-waves (*Sec 4.2)*. They were picked iteratively to increase precision. Figures 6.7 & 6.8 show recorded signals with varying degree of S/N ratio.

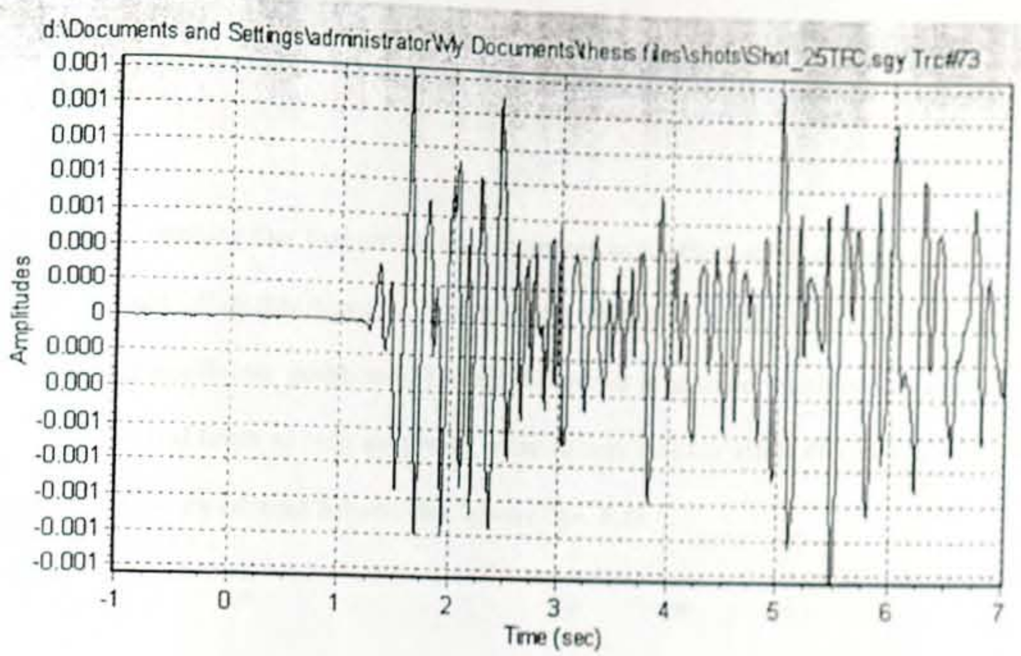

Fig 6.7 High S/N ratio signal recorded from SP 25

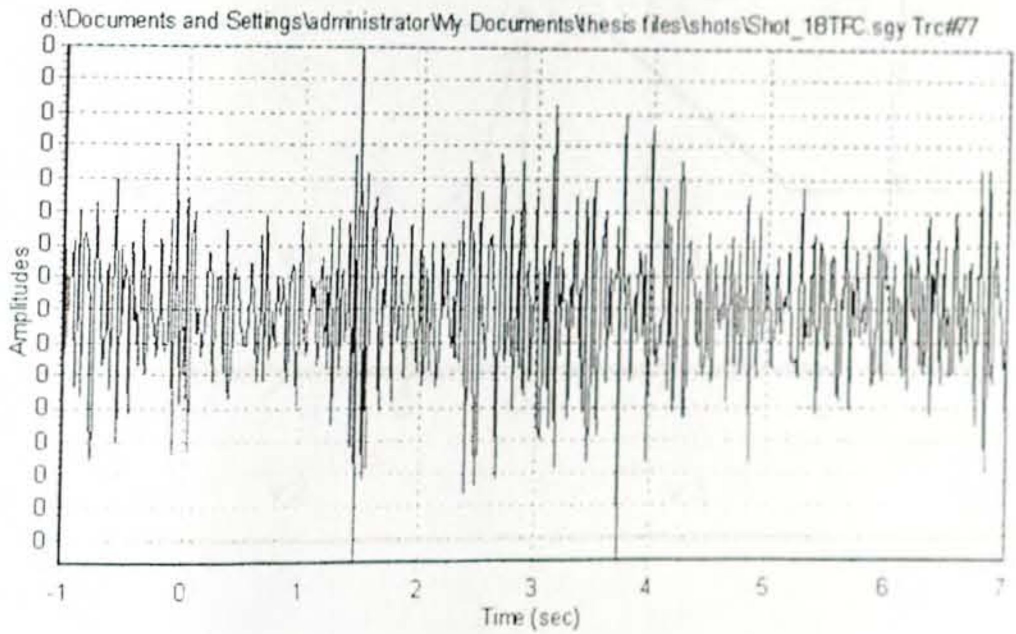

Fig 6.8 Low S/N ratio signal recorded from SP 18

6.2.1 Raw traces

With the understanding that first arrival time increases with offset, some of the seismic arrivals *(Fig 6.1 to 6.6)* do not follow this principle. The scientific rational is mostly controlled by the difference in altitudes between adjacent geophones. Though difference in altitude which is also known as *statics*, controls the arrival times at each geophone, other factors include offset distance between geophone pairs and the velocity contrast between the layers *(Eqn. 6.2)*.

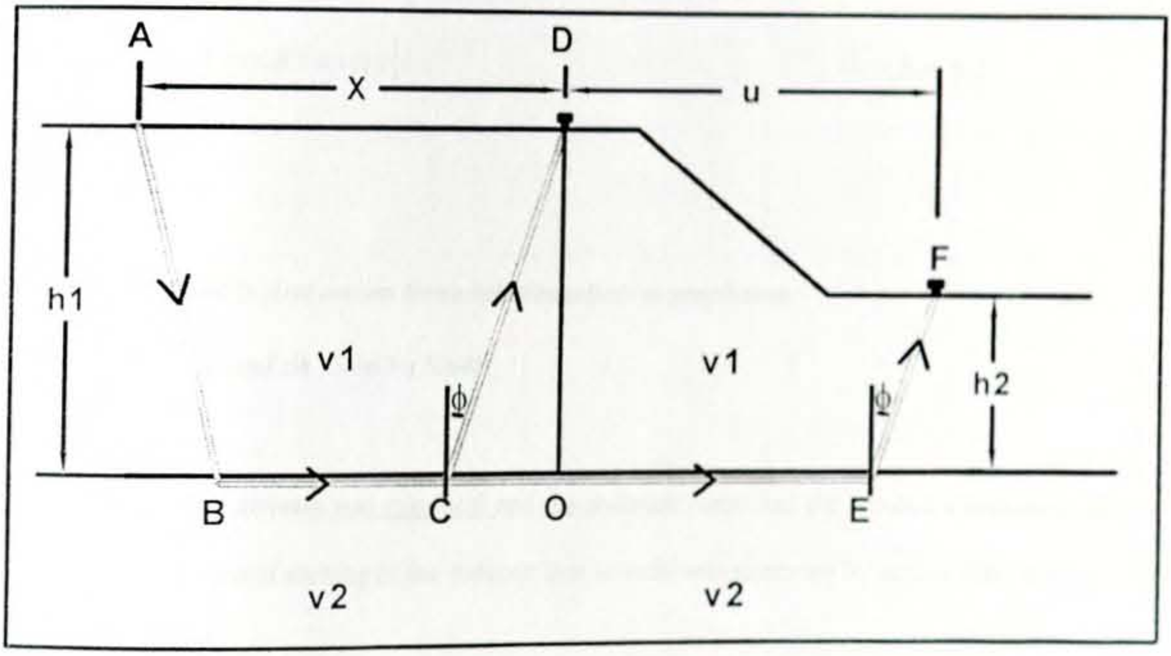

Fig 6.9 Diagram showing geophones placed at different elevations

ϕ = Critical angle of incidence

h_1, h_2 = height from the surface to the refractor

v_1 & v_2 = seismic velocities of layer 1 & 2 respectively

x = distance from shot to 1st geophone

u = distance between consecutive pair of geophones

t_1= time taken for the seismic wave to travel from the shot to the 1st geophone

t_2=time taken for the seismic wave to travel from the shot to the 2nd geophone

Δt= difference in time between consecutive pair of geophones

$$\Delta t = \frac{1}{v1}\left[(h2 - h1)\cos\phi + u\sin\phi\right] \qquad \text{Eqn 6.2}$$

Where

Δt is the difference in first arrival times between adjacent geophones

$\Delta t < 0$ iff. $\{h_2 < h_1$ and $\Delta h\ Cos\phi > u\ Sin\phi\}$

Picking of the first arrivals was graphical and the software identifies the seismic traces to be space-time referenced. Actual picking of the reduced first arrivals was executed by screen digitizing the raw traces (*Appendix 5).*

This data was later converted to an excel format to increase manipulation. The major steps that were done here are;

1) Conversion of the *.txt to *.xls format.

2) Converting the rational trace numbers as recognized by the picking software to integral trace numbers *(Appendix 5)*.

3) Assigning true offset value from each shot to each trace

4) Converting the picked reduced first arrival times to their actual arrival times using equation 6.1 (*Appendix 6)*.

6.2.2 Shot to geophone configuration

The software Gremix has a certain configuration which it would attain its shot-geophone nomenclature (*Fig 6.10)*. It recognizes the far end shots (C & D), end shots (A & B) and center shot (E) based on the offset data we feed it.

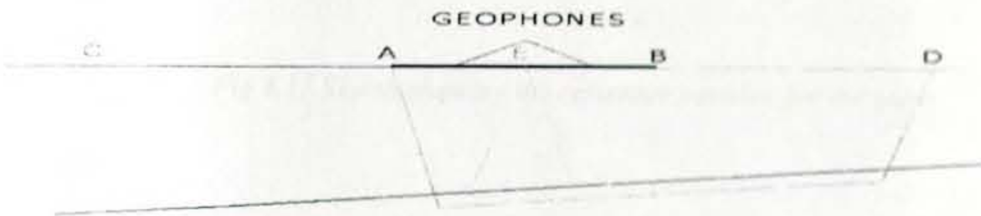

Fig.6.10 Sketch showing the nomenclature of GREMIX

When a reference position with a value of zero is given, the inverting software "Gremix" automatically assigns positive values to the geophones on the right of this relative position and negative values to the left *(Fig 6.11)*. SP 14 *i.e* the far end shot designated by the letter "C" was assigned to be the reference point in this study hence, there are no negative values that have been recognized as offsets (*Appendix 6)*.

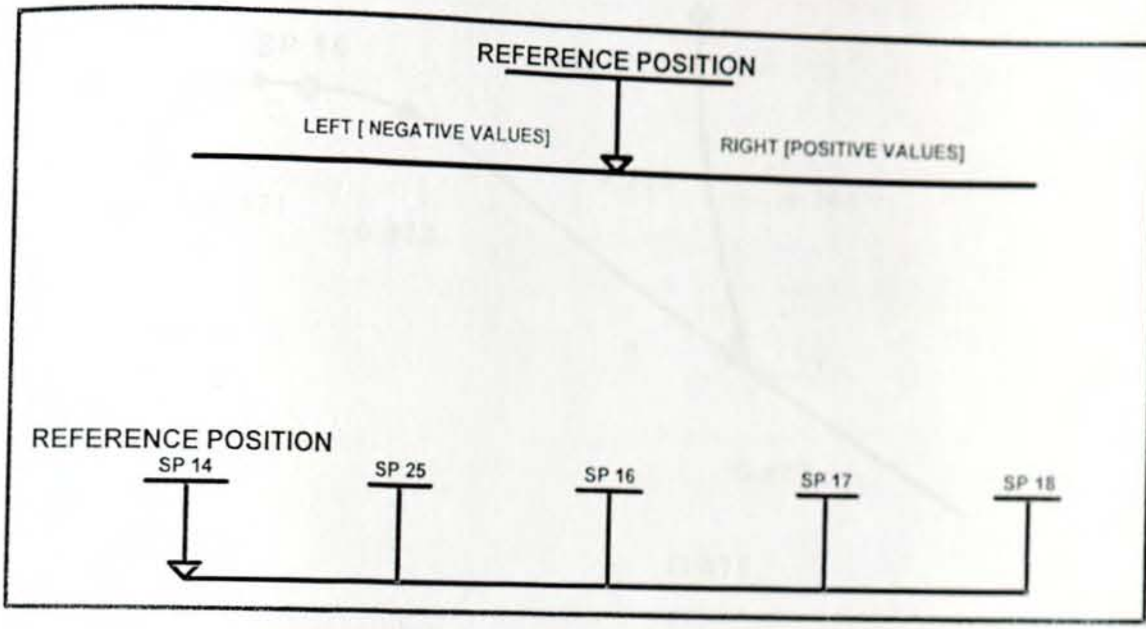

Fig 6.11 Sketch showing the reference position for the input

The P-wave fist arrival time and offset values of Geophone no. 72 –76 were taken with respect to SP 15 and that of geophone no. 77 – 158 were given values with respect to SP 25 (*Appendix 6)*. This was performed to increase the precession of the reciprocal time *(Fig 6.12)*.

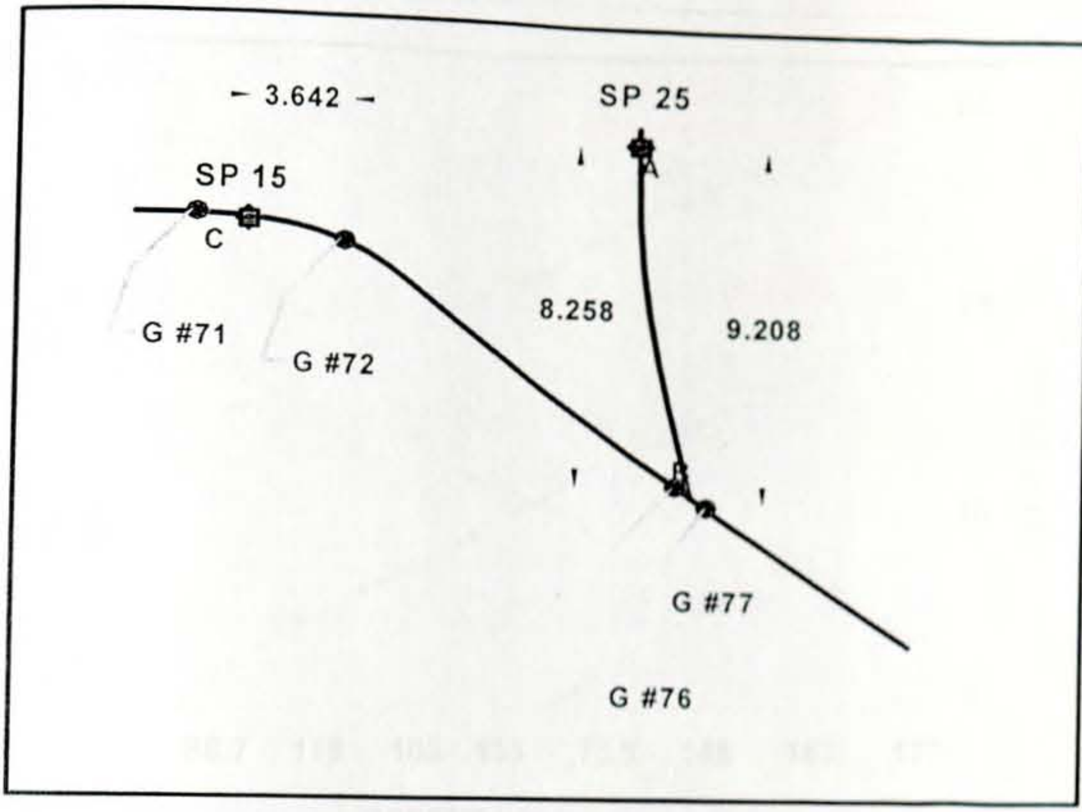

Fig 6.12 Sketch showing the placement of SP15 and SP25 with respect to each other

6.2.3 Data inversion

After feeding the data into the processing software Gremix, which is an interpretation software, incorporating the methods of the GRM (*Sec 4.3)*, it automatically performs static corrections based on the elevation parameters of each geophone (*Fig 6.13)*.

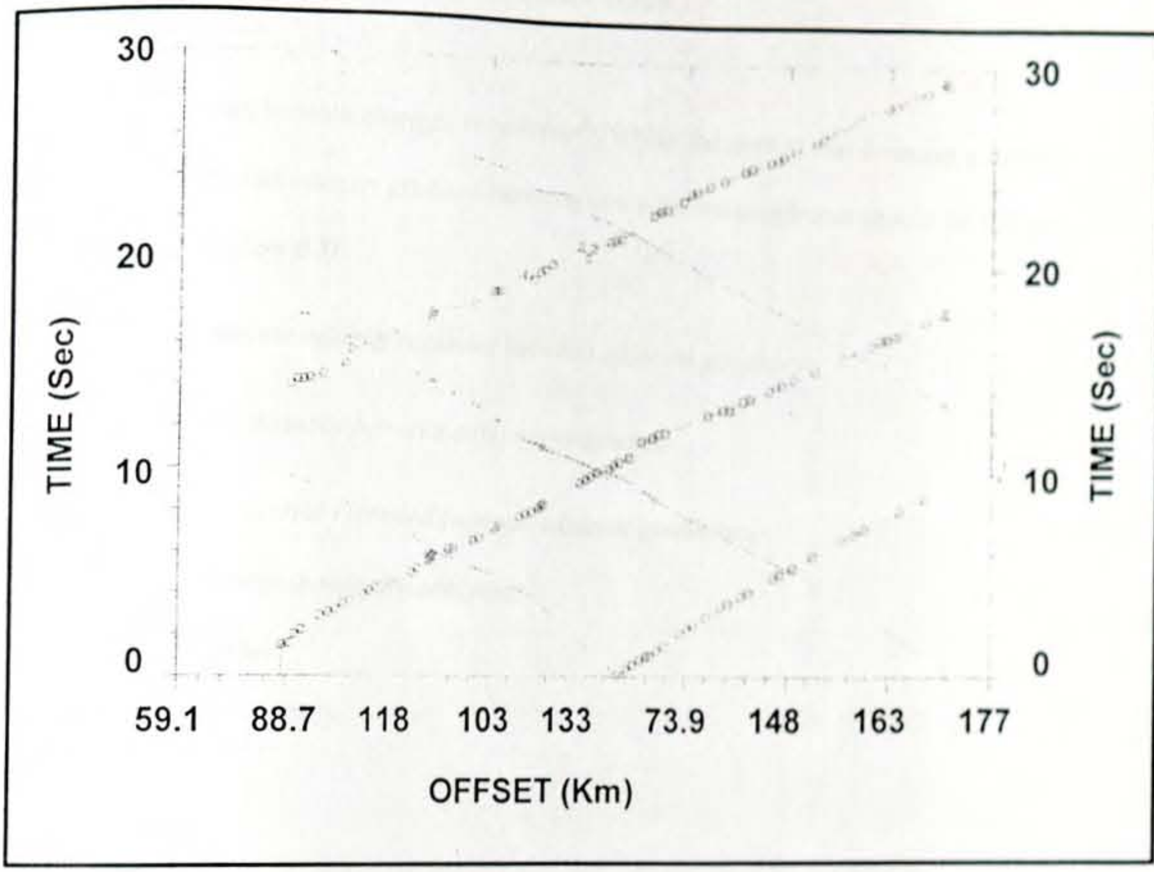

Fig 6.13 Static corrected arrival times

6.2.4 Techniques of identifying velocity changes

Different techniques were used when trying to identify the velocity changes with depth. Basically these techniques were namely:

a) Velocity Gradient Difference Analysis *(VGDA)*

b) Mirror image analysis *(MIA)*

6.2.4.1 *Velocity Gradient Difference Analysis* (VGDA)

Unless the geology beneath changes very abruptly within the pretext that it causes a significant arrival velocity changes, the velocity gradient between two adjacent geophones should be the same or more or less the same. (*Eqn 6.3)*

v_n = *Apparent seismic velocity recorded between adjacent geophones*

$x_n - x_{n+1}$ = *Offset distance between adjacent geophones*

$t_n - t_{n+1}$ = *Time of arrival recorded between adjacent geophones*

VGDA = Δv = *Change in velocity analyzed*

n = *Geophone number*

$$v_n = \frac{x_n - x_{n+1}}{t_n - t_{n+1}}$$

$$\Delta v = v_{n+1} - v_n$$

Eqn 6.3

In an ideal case Δv should give us a value of zero when there is no change in velocity or it should give us a value different from zero when there is a change in velocity between adjacent geophones. With this assumption, *VGDA (Fig 6.14)* was calculated for each geophone from each shot.

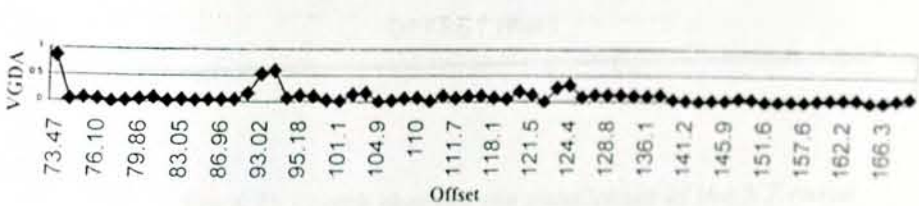

Fig 6.14 VGDA from SP 25

Looking at figure 6.14, it shows a clean agreement with the assumption above. Hence the only points deviating from the zero *VGDA* would be an indication of a change in seismic velocity.

6.2.4.2 Mirror image analysis

In this method the assumption basically lied on the precondition that refractors do not dip significantly, otherwise the intercept time will vary significantly. The seismic waves coming from the same refractor would manifest themselves by being aligned on the travel time curve. This line is referred to as the parallelism line *(Fig 6.15)*.

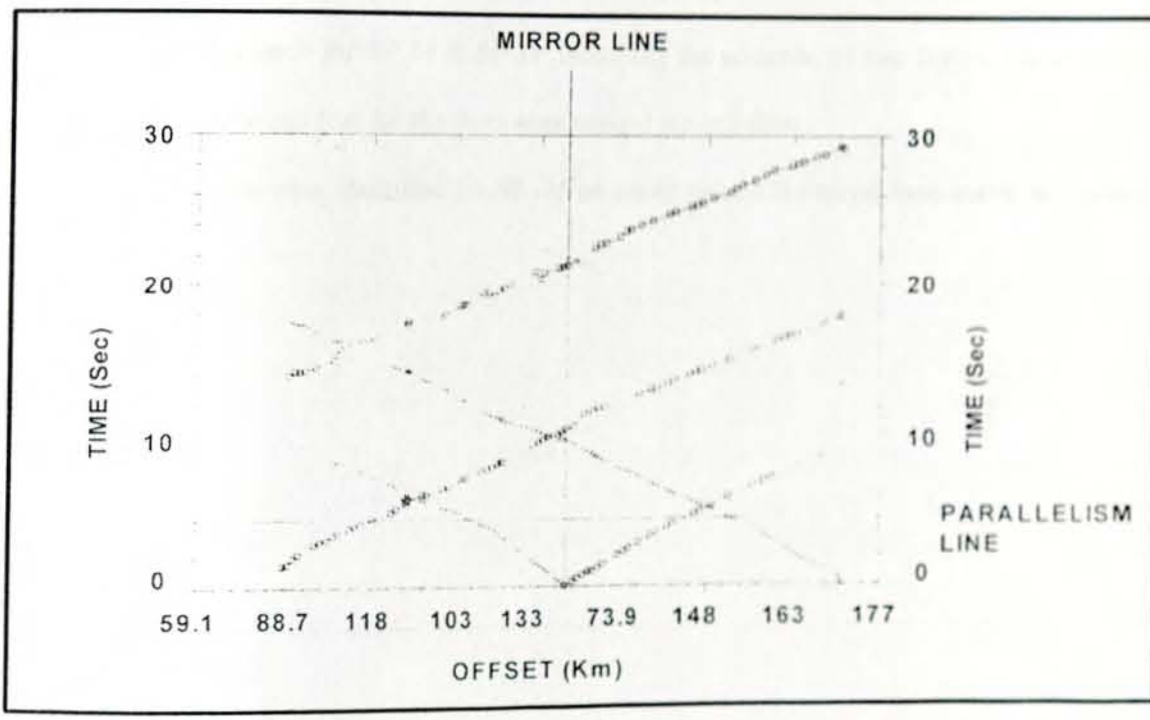

Fig 6.15 Sketch showing the parallelism of the XT curve

Layer assignments were carried out iteratively using the techniques discussed earlier, which were assisting as controls for the procedure (*Fig 6.16)*. Reciprocal times were checked before the inversion process was carried out.

The inversion process was carried out using Gremix. Optimum XY values were determined for each velocity analysis and time depth function. The time depth was later converted into actual depth with the assignment of the true velocity to each layer.

The layer assignment shown in Figure 6.16 were

- ✓ Three refractors each for SP 25 & SP 17, indicating the presence of four layers
- ✓ One refractor each for SP 14 & SP 18, indicating the presence of two layers. These layers would be three and four for the shots were beyond the end shots.
- ✓ Two refractors were identified for SP -16 on either side of the travel time curve, indicating three layers.

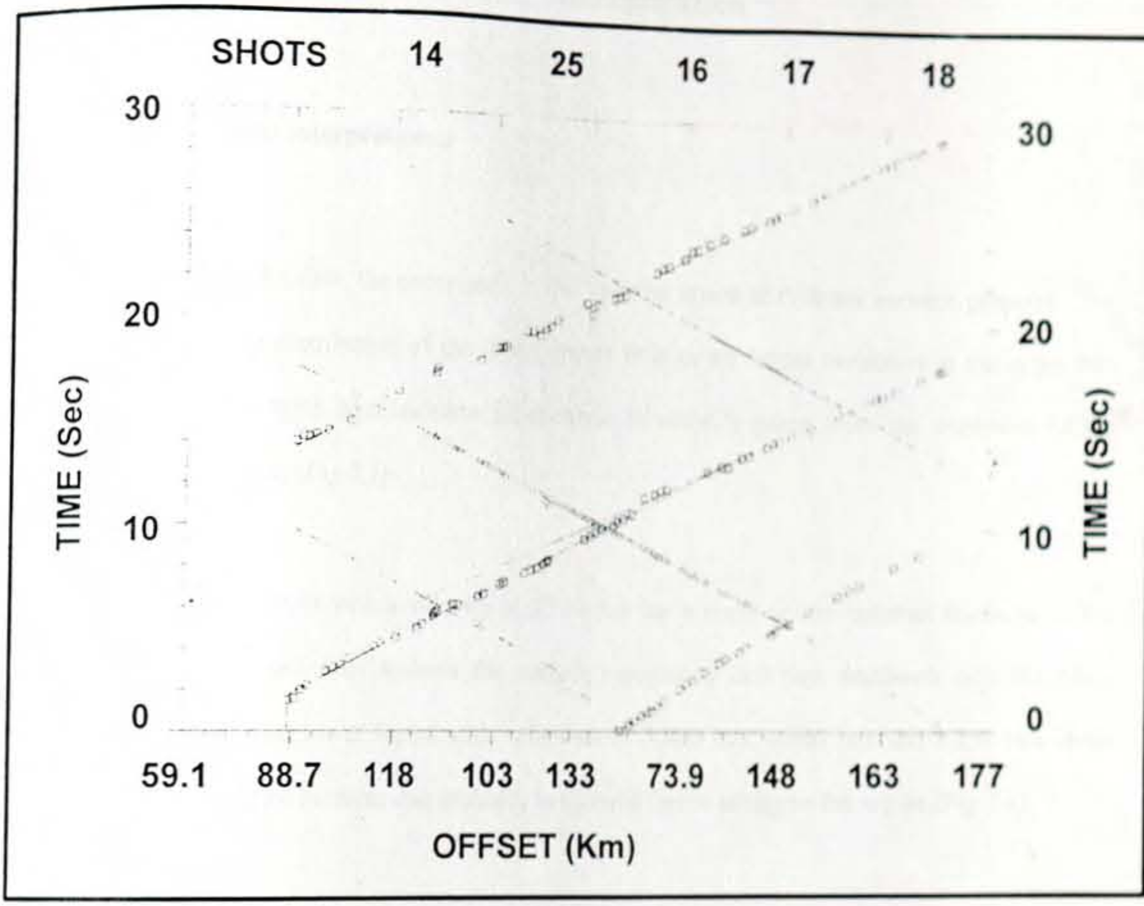

Fig 6.16 Assigned arrival curves

The seismic model of the eastern plateau using the GRM method of inversion was then finally produced. The output from the inversion software indicates four layers to a max depth of 10 km.

7. Interpretation

7.1 Geophysical interpretation

After inverting the data, the geoseismic model had four layers of different acoustic property. The seismic velocity distribution of the layers shows little or no lateral variations in the upper two layers. But the third layer exhibits an increase in velocity going from the northwest to the southeast direction (*Fig.7.1*).

The upper most layer with a velocity of 2,700 m/s has a more or less constant thickness in the studied area. It generally follows the surface topography and dips northwest into the Main Ethiopian rift. The lower layers with velocities of 3,900 m/s, 5,800 m/s and 6,259 m/s show undulating refractor surfaces due probably to tectonic forces acting on the region *(Fig 7.1)*.

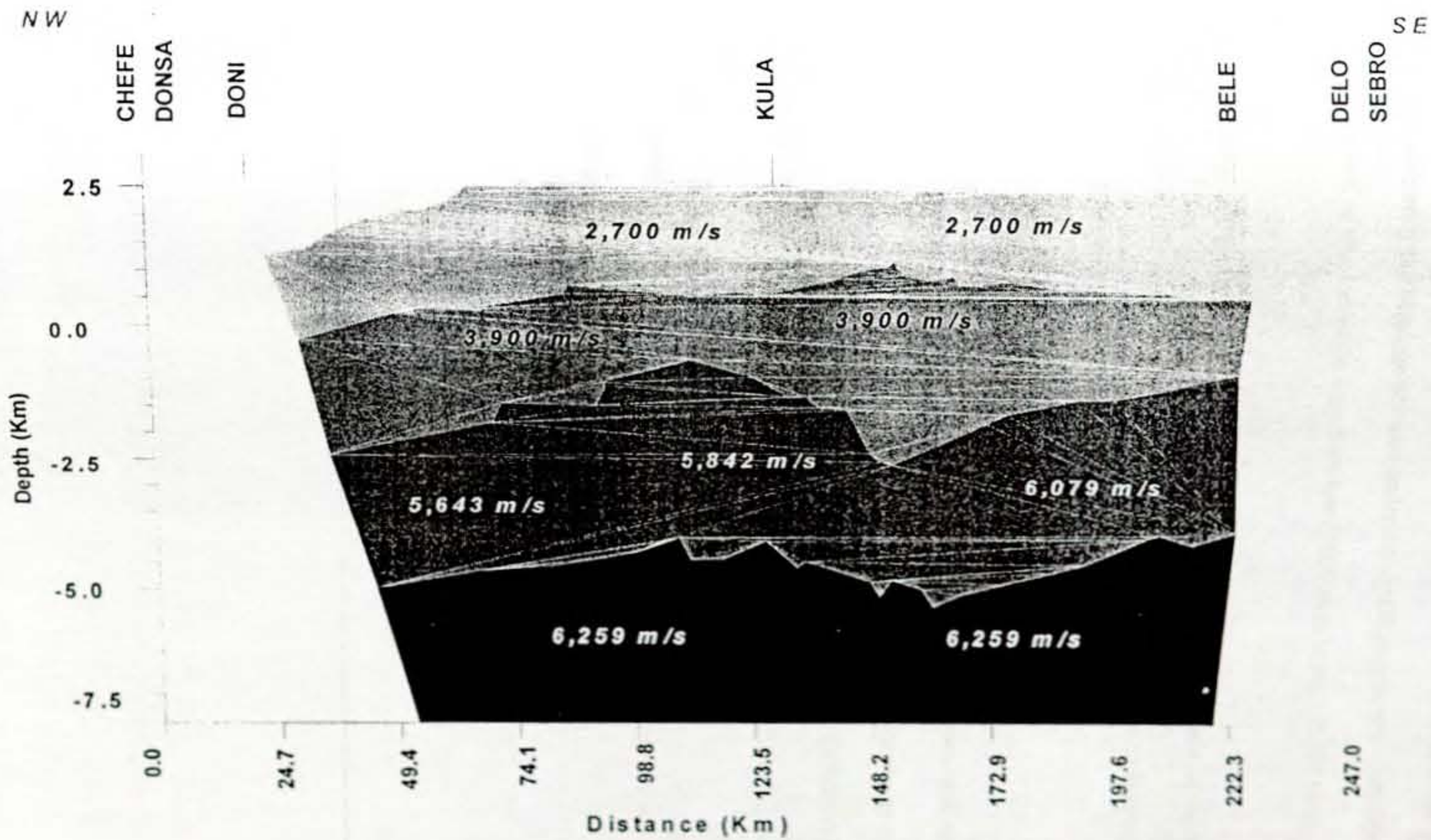

Fig 7.1 Seismic model beneath the Eastern plateau

7.2 Geological interpretation

The geology of the study area (*Chapter 2)* is characterized by the Cenozoic era on top where it is divided into primarily the Miocene volcaics underlain by Oligocene pre – rift flood volcanics The seismic velocities of this formation vary from low (1000 m/s) to high (6500 m/s).

This era is underlain by the Mesozoic sediments, which are of considerable thickness where the major lithologies in this period are limestone & Sand stone. The P-wave velocities in rocks of this period vary from low (1500 m/s) to high (6000m/s).

Beneath all the formations lies the basement complex on which all known rock types rest. They are formed under high pressure and temperature giving them a higher density as compared to the other rock types. The P – wave velocities in this complex vary from low (3000 m/s) to high (7000 m/s), (*Appendix 7)*.

Knowing the geological setting of the study area coupled with the determined seismic velocities (*Appendix 7)*, the geological section interpreted is shown in the figure 7.2.

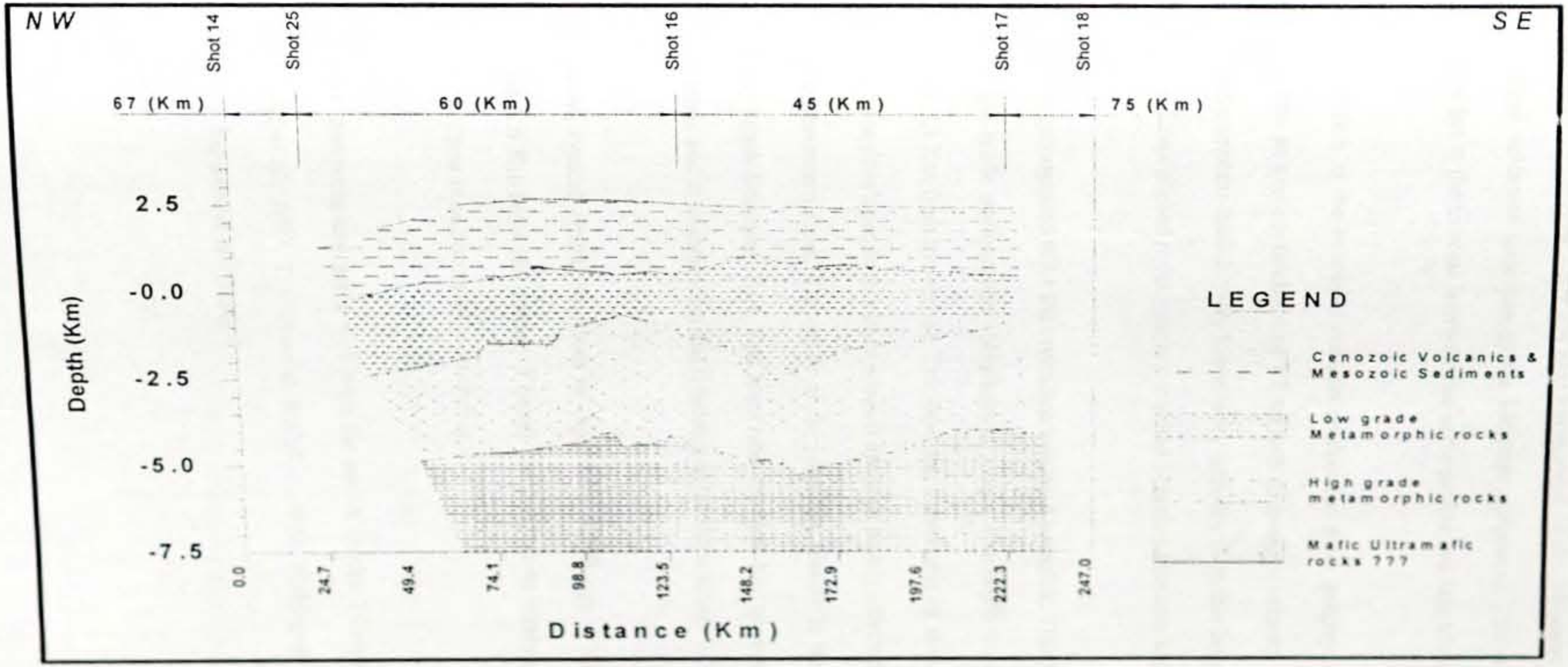

Fig 7.2 Geological section of the study area

The first layer to a depth of around 1.3 – 2.0 km is comprised of the Miocene volcanics and the Oligocene pre-rift flood volcanics underlain by the Mesozoic sediments. The stratigraphy for this layer follows like wise but at the extreme southeast end of the profile, we find Mesozoic outcrops.

The second layer therefore is the basement complex as deduced from geophysical and geological evidences. This layer has an average thickness of 2.2 km with an average velocity of 3,900 m/s. With regard to the basement complex; the relatively low velocity recorded from this layer could most likely represent low-grade metamorphosed rocks mainly composed of meta sediments and or volcanics.

The third layer has been recognized to be the crystalline basement complex. This high velocity could be attributed to the high-grade metamorphic rocks such as gneiss. The depth to the top of this layer varies from 3.3 Km to 5.3 Km from the surface. This layer has a thickness of about 2.2 – 3.2 Kms. A horst like feature has been developed in this layer where it has been highly affected by the Assela-Sire border fault on its northwestern flank. The center of the horst like feature is only 50 km from the eastern margin of the Main Ethiopian Rift. This horst like structure has no anomalous P – Wave velocity from its environs and is an indication that it belongs to the same layer.

The fourth layer shows typical crustal velocities of more than 6,200 m/s. This layer starts at an approximate depth of 6.6 Km from the surface. Though this layer most likely represents rocks of mafic ultramafic nature, there is no concrete evidence (*Fig 7.2*).

The above geological interpretations agree well with the earlier works. (*Gebreyohanes Habtezgi 1984; Hambisa Gobena et al., 1997; T. Chernet & W.K.Hart, 1999; Woldegabriel et al., 1999; M Bocaletti et al., 1999; K.Keranen et al., 2004*).

8. Conclusions and Recommendation

8.1 Conclusions

From the results obtained in this study the following conclusions can be made

Cabeless recording Texans have been found very effective in carrying out seismic experiments of this scale.

The technique that was used to determine the break points during layer assignments has produced very good results.

Though the data quality is very high with very good energy propagation across the entire length of the profile, the uneven explosive distribution inside the boreholes has caused a slight problem in adjusting amplitude gain when performing data processing.

The study indicates the presence of four layers beneath the eastern plateau down to a maximum depth of 10 kilometers. These layers from top to bottom have average velocities of 2,700 m/s, 3,900 m/s, 5,800 m/s and 6,300 m/s at depth of 2.0 km, 5.0 km, and 7.0 km.

By correlation with the known geology and using deterministic P-wave velocities, the first layer comprises the Cenozoic volcanics and sediments of the Mesozoic sequences. The second and third layer on the other hand is the low grade and high-grade metamorphic rocks. The fourth layer shows typical crustal velocities greater than 6,200-m/s. This layer could most likely be interpreted as to be comprised of the mafic – ultra mafic rocks.

All the layers dip in the northwest direction which could most likely be attributed to the Assela-Sire border fault located on the eastern margin of the Main Ethiopian rift. This same border fault is the most probable reason for the formation of the horst like structure found in the third layer. However, the formation of this structure could also be attributed to compressional tectonic forces acting along the profile.

The center of the horst like structure is located in a locality known as Hamda Diksis. The depth to the top of this horst is 3.3 Km from the surface. The maximum thickness is 3.7 Km and is located 13 km northwest from shot 16, Kula.

8.2 Recommendations

Geophysical study based on refraction seismic methods to the study area is the first of its kind. Hence this work is just a beginning for further detailed studies; therefore further refinements to this work can be made. Based on the out come of this study, I suggest the following recommendations

1) To differentiate between the different flows of volcanic units and isolate the Quaternary sediments, as well as to map the structural features, finer sampling of wave field is needed.
2) Gravity surveying should be carried out to constrain seismic inversion results.
3) Amplitude studies of the first arrivals should also be undertaken to understand the attenuating behavior of the rocks.
4) Reflection seismic methods be employed to differentiate between Cenozoic volcanics and the Mesozoic sediments and to identify deep seated structures.

Reference:

1) Alan E. Musset and M. Aftab Khan, 2000, Looking into the earth: An introduction to geological geophysics, Cambridge University Press, Cambridge, Great Britain.

2) Dobrin M.B., 1976, Introduction to Geophysical prospecting 3rd edition, McGraw-Hill book company New York.

3) Eagle phase III; The controlled source seismic project, June 2003, Fieldwork report.

4) G. Wolde Gabriel et al.... 1999, Temporal relations and geochemical features of felsic volcanism in the central sector of the Main Ethiopian Rift: Acta Vulcanologica - vol.11 (1) p.53-67.

5) G.M.Di Paola, 1972, The Ethiopian rift valley (Between 7° 00' and 8° 40' lat North): Bulletin Volcanologique, p.517-560.

6) Gebreyohanes Habtezgi, December 14, 1984, Stratigraphic succession of the upper second and third order tributaries of the Wabeshebele River.

7) Hambisa Gobena et al.... 1997, A.A, Geology of the Dodola area.

8) K. Karanen, S.L. Klemperer et al.... 2004, 3D seismic Imaging of a proto-ridge axis in the Main Ethiopian Rift, The east Afrcan Rift system: Geodynamics, Resources and Environment.

9) M.Boccaletti, et al.... 1999, Pliocene-Quaternary volcanism and faulting in the northern main Ethiopian Rift (with two geological maps at scale 1:50,000): Acta Vulcanologica - Vol.11 (1) p.83 -97.

10) Paul A. Mohr, 1971, The Geology of Ethiopia

11) Palmer, D., 1981, An introduction to the generalized reciprocal method of seismic refraction interpretation: Geophysics. 46, 1508-1518

12) Palmer, D., February 2003. Application of amplitude in shallow seismic refraction inversion. ASEG 16th Geophysical conference and exhibition, Adelaide.

13) Robert S. Carmichael, 1989, Physical properties of rocks and minerals, CRC press Inc. Florida, United States.

14) Robert W. Lankston, 1989, the seismic refraction method: A viable tool for mapping shallow targets into the 1990s: Geophysics, ??, 1535-1542.

15) Robinson, E.S., & Coruh, C., 1988, Basic Exploration Geophysics, John Wiley & Sons, Newyork.

16) T. Chernet, W.K.Hart, 1999, Petrology and geochemistry of volcanism in the northern main Ethiopian Rift-Southern Afar transgression region: Acta Vulcanologica–Vol.11 (1) P.21-41.

17) Telford, W.B, 1978, Applied Geophysics, Cambridge University Press, Cambridge, Great Britain.

18) V.Kazmin, 1972, Geology of Ethiopia (Explanatory note to the geological map of Ethiopia 1:2,000,000).

19) V.Kazmin, May 1979, Stratigraphic and correlation of volcanic rocks in Ethiopia.

20) William Lowrie, 1997, Fundamentals of Geophysics, Cambridge University Press, Cambridge, Great Britain.

APPENDIX

APPENDIX 1 – GEOPHONE STATION, LOCATION AND ALTITUDE

Station	Altitude	Easting	Northing	Zone
1250	1300	564439.4	936347.4	37N
1251	1312	564889.0	935518.1	37N
1253	1339	566050.7	934159.3	37N
1254	1361	566823.9	933439.3	37N
1255	1380	567420.9	932500.9	37N
1256	1637	567628.4	931231.7	37N
1257	1752	568495.6	930668.4	37N
1259	1868	570079.1	929371.7	37N
1260	1938	570466.5	928479.8	37N
1261	1976	571310.5	927943.0	37N
1263	2110	573204.7	926688.2	37N
1264	2093	574362.8	926516.0	37N
1265	2109	574071.7	925624.6	37N
1267	2291	574049.1	923340.4	37N
1268	2451	573922.3	922188.5	37N
1269	2529	574308.3	921191.4	37N
1271	2570	573053.8	919268.8	37N
1272	2579	572399.4	918500.4	37N
1273	2576	571611.4	917511.7	37N
1275	2609	573494.3	915973.8	37N
1276	2633	574476.6	915932.8	37N
1277	2613	575042.9	914989.2	37N

1279	2653	575905.0	913294.4	37N
1280	2693	576021.8	912312.2	37N
1282	2704	576799.3	910661.2	37N
1283	2686	576512.2	909695.7	37N
1284	2686	576081.6	908722.2	37N
1286	2682	577055.7	906860.0	37N
1287	2672	577511.8	905923.7	37N
1288	2663	577974.6	905028.2	37N
1289	2659	578461.4	904179.0	37N
1291	2666	578376.3	902926.6	37N
1292	2655	577933.9	902039.5	37N
1293	2637	577174.4	901127.3	37N
1294	2635	577639.9	900235.8	37N
1295	2626	578112.5	899346.2	37N
1297	2587	577593.8	897561.5	37N
1298	2622	576431.6	897211.4	37N
1300	2605	576204.0	895909.1	37N
1302	2595	575675.8	893522.4	37N
1303	2588	575681.5	892475.4	37N
1304	2570	575432.0	891508.3	37N
1305	2568	575746.9	890436.0	37N
1307	2542	576162.5	888738.8	37N
1308	2531	575863.0	887776.2	37N
1309	2506	575782.5	886783.5	37N
1311	2507	575476.8	885020.1	37N

1312	2503	575535.8	884132.9	37N
1313	2491	575611.8	882974.4	37N
1314	2476	575836.2	881986.3	37N
1316	2477	577060.1	881968.4	37N
1317	2483	577955.2	881926.5	37N
1318	2488	578911.7	881961.3	37N
1323	2463	582461.5	877702.2	37N
1325	2468	583506.5	876193.2	37N
1326	2486	584195.3	875266.8	37N
1327	2470	584863.2	874510.3	37N
1328	2469	585634.1	873782.2	37N
1330	2450	587017.6	872330.0	37N
1331	2436	587570.0	871480.4	37N
1332	2441	588282.9	870837.0	37N
1334	2496	589513.8	869422.1	37N
1335	2499	590346.8	868857.6	37N
1336	2493	591144.2	868348.0	37N
1338	2480	592668.7	867067.4	37N
1339	2476	593478.3	866558.8	37N
1341	2492	595345.5	865266.3	37N
1342	2466	596181.5	864697.6	37N
1343	2461	596969.1	863896.1	37N
1345	2478	598086.0	862034.6	37N
1347	2480	599891.7	861076.4	37N
1349	2481	601357.5	860255.4	37N

1350	2476	602332.5	859974.1	37N
1352	2457	604251.6	859656.3	37N
1353	2464	605236.3	859180.8	37N
1354	2446	605983.3	858462.1	37N
1355	2435	606684.9	857719.0	37N
1357	2443	608224.8	856236.2	37N
1358	2443	609401.3	855161.8	37N
1361	2470	611928.7	853697.6	37N
1362	2442	613326.2	854101.3	37N
1363	2427	614429.7	854307.9	37N
1364	2466	615366.9	854297.1	37N
1365	2468	616621.3	854204.9	37N
1367	2484	618418.3	853052.2	37N
1368	2476	619440.9	852424.2	37N
1369	2479	620083.2	851850.9	37N

APPENDIX 2 - OFFSET OF EACH GEOPHONE FROM EACH SHOT

Station	Offset from SP 14 (Km)	Offset from SP 15 (Km)	Offset from SP 25 (Km)	Offset from SP 16 (Km)	Offset from SP 17 (Km)	Offset from SP 18 (Km)	Texan- Texan distance (Km)
	SHOT						
	|	SHOT					
1250	73.472	3.642		53.973	98.663	173.727	0.835
1251	74.307	4.53		53.075	97.774	172.86	0.963
1253	75.27	5.525		52.073	96.763	171.869	0.836
1254	76.106	6.373		51.227	95.897	171.014	0.919
1255	77.025	7.292		50.319	94.953	170.08	1.786
1256	78.811		9.208	48.746	93.19	168.296	1.052
1257	79.863		9.785	47.89	92.177	167.256	1.105
1259	80.968		10.664	46.854	91.058	166.14	1.08
1260	82.048		11.922	45.57	89.866	165.007	1.001
1261	83.049		12.487	44.864	88.934	164.031	2.026
1263	85.075		13.925	43.345	87.011	162.039	0.924
1264	85.999		14.868	42.409	86.044	161.092	0.959
1265	86.958		15.551	41.777	85.159	160.159	2.203
1267	89.161		17.249	40.362	83.13	158.019	0.909
1268	90.07		17.791	40.13	82.418	157.192	0.466
1269	90.536		18.533	39.251	81.775	156.644	1.687
1271	92.223		20.7	36.968	79.799	154.831	0.793
1272	93.016		21.775	35.823	78.862	153.983	1.003

1273	94.019	22.837	34.808	77.811	152.962	0.676
1275	94.695	24.406	32.967	76.818	152.213	0.192
1276	94.887	25.039	32.263	76.517	152.014	0.288
1277	95.175	25.893	31.376	76.124	151.741	2.374
1279	97.549	27.726	29.644	73.8	149.357	0.64
1280	98.189	27.975	29.543	73.234	148.711	1.09
1282	99.279	29.026	28.578	72.135	147.621	1.866
1283	101.145	30.883	26.871	70.241	145.759	0.849
1284	101.994	31.865	25.889	69.349	144.917	1.779
1286	103.773	33.66	24.256	67.542	143.147	0.593
1287	104.366	34.523	23.28	66.895	142.581	0.513
1288	104.879	35.366	22.297	66.338	142.113	2.08301
1289	106.96201	37.408	20.469	64.246	140.053	1.023
1291	107.98501	38.428	19.567	63.218	139.045	0.997
1292	108.98201	39.411	18.723	62.218	138.061	0.973
1293	109.95501	40.358	17.943	61.242	137.098	0.96
1294	110.91501	41.547	16.692	60.276	136.203	0.464
1295	111.37901	42.303	15.75	59.823	135.821	0.302
1297	111.68101	43.022	14.756	59.566	135.646	1.003
1298	112.68401	43.995	13.922	58.571	134.664	0.997
1300	113.68101	44.966	13.112	57.584	133.69	1.181
1302	114.86201	46.599	11.267	56.525	132.715	-0.357
1303	114.50501	46.719	10.793	57.016	133.251	0.97
1304	115.47501	47.965	9.481	56.185	132.451	1.723
1305	117.19801	50.236	7.086	54.808	131.103	0.895

1273	94.019		22.837	34.808	77.811	152.962	0.676
1275	94.695		24.406	32.967	76.818	152.213	0.192
1276	94.887		25.039	32.263	76.517	152.014	0.288
1277	95.175		25.893	31.376	76.124	151.741	2.374
1279	97.549		27.726	29.644	73.8	149.357	0.64
1280	98.189		27.975	29.543	73.234	148.711	1.09
1282	99.279		29.026	28.578	72.135	147.621	1.866
1283	101.145		30.883	26.871	70.241	145.759	0.849
1284	101.994		31.865	25.889	69.349	144.917	1.779
1286	103.773		33.66	24.256	67.542	143.147	0.593
1287	104.366		34.523	23.28	66.895	142.581	0.513
1288	104.879		35.366	22.297	66.338	142.113	2.08301
1289	106.96201		37.408	20.469	64.246	140.053	1.023
1291	107.98501		38.428	19.567	63.218	139.045	0.997
1292	108.98201		39.411	18.723	62.218	138.061	0.973
1293	109.95501		40.358	17.943	61.242	137.098	0.96
1294	110.91501		41.547	16.692	60.276	136.203	0.464
1295	111.37901		42.303	15.75	59.823	135.821	0.302
1297	111.68101		43.022	14.756	59.566	135.646	1.003
1298	112.68401		43.995	13.922	58.571	134.664	0.997
1300	113.68101		44.966	13.112	57.584	133.69	1.181
1302	114.86201		46.599	11.267	56.525	132.715	-0.357
1303	114.50501		46.719	10.793	57.016	133.251	0.97
1304	115.47501		47.965	9.481	56.185	132.451	1.723
1305	117.19801		50.236	7.086	54.808	131.103	0.895

1307	118.09301		51.274	6.038	54.052	130.347	0.69
1308	118.78301		52.194	5.085	53.552	129.839	1.078
1309	119.86101		53.301	3.997	52.584	128.862	1.67
1311	121.53101		55.043	2.322	51.117	127.371	0.667
1312	122.19801		55.951	1.336	50.702	126.923	0.817
1313	123.01501		56.925	0.344	50.106	126.29	
				SHOT			
1314	124.38401		58.634	1.464	49.216	125.306	0.797
1316	125.18101		59.522	2.328	48.621	124.663	1.046
1317	126.22701		60.682	3.475	47.852	123.822	0.97
1318	127.19701		61.69	4.457	47.086	122.996	0.622
1323	127.81901		61.874	4.642	46.091	122.075	0.485
1325	128.30401		62.053	4.993	45.356	121.387	0.457
1326	128.76101		62.179	5.442	44.622	120.706	1.001
1327	129.76201		62.95	6.486	43.514	119.609	2.477
1328	132.23901		65.133	9.001	41.039	117.105	1.118
1330	133.35701		66.224	10.096	40.036	116.061	0.887
1331	134.24401		67.053	10.982	39.201	115.2	1.83
1332	136.07401		68.755	12.814	37.468	113.414	1.148
1334	137.22201		69.814	13.967	36.37	112.283	0.997
1335	138.21901		70.708	14.977	35.383	111.275	1.024
1336	139.24301		71.601	16.026	34.332	110.213	1.959
1338	141.20201		73.356	18.021	32.371	108.214	1.014
1339	142.21601		74.321	19.031	31.44	107.234	0.92
1341	143.13601		75.13	19.976	30.495	106.277	1.855

1342	144.99101		76.832	21.855	28.689	104.409	0.916
1343	145.90701		77.608	22.816	27.688	103.416	0.86
1345	146.76701		78.331	23.725	26.734	102.475	1.896
1347	148.66301		80.011	25.689	24.764	100.485	0.862
1349	149.52501		80.746	26.605	23.81	99.545	2.096
1350	151.62101		82.573	28.816	21.543	97.293	0.933
1352	152.55401		83.389	29.804	20.531	96.289	1.101
1353	153.65501		84.412	30.927	19.448	95.168	2.171
1354	155.82601		86.546	33.054	17.584	93.089	1.794
1355	157.62001		88.084	34.99	15.534	91.102	1.489
1357	159.10901		89.383	36.593	13.864	89.471	0.78
1358	159.88901		90.015	37.484	12.857	88.557	1.34
1361	161.22901		91.055	39.083	11.014	86.94	0.948
1362	162.17701		91.885	40.126	9.924	85.9	1.013
1363	163.19001		92.844	41.159	8.926	84.866	1.013
1364	164.20301		93.811	42.182	7.957	83.842	2.096
1365	166.29901		95.8	44.319	5.96	81.705	1.559
1367	167.85801		97.275	45.918	4.524	80.107	2.655
1368	170.51301		99.691	48.772	1.967	77.268	0.48
1369	170.99301		99.95	49.545	0.521	76.565	
					SHOT	|	
						SHOT	

APPENDIX 3 - WELL LOG OF SP 15

Project:	*EAGLE*		**Drilling method:**	*Air Rotary/DTH*
Client:	*Leicester University*		**Rig type:**	*TH 60*
Location:	*Doni A*		**Coordinate: N**	*942514.5*
Shot hole designation:	*SP 15*		**:E**	*562852.55 | 37N*
Shot hole No.:	*SH 1*		**Altitude:**	*1226*
Casing depth (m):	*42.20*		**Inclination:**	*Vertical*
Casing Diameter:	*8.5"*		**SWL:**	*18.95 m*

Well lithologic log

Depth (m)	Section	Lithologic description
0 -2		Olive gray, silt (tuff)
2-3.		Olive gray, sand silt (tuff) with few rounded gravel
3-6.		Conglomerate
6-10.		Conglomerate, mixed with pale green to white pumice
10-12.		Pale green pumice
12-13.		Same as10 -12, mixed with gray, slightly weathered ignimbrite
13-19		Gray slightly weathered ignimbrite
19-21		Brownish gray, gravely and sandy silt
21-26		Conglomerate
26-30		Brownish gray, sandy and gravely silt
30-32		Brownish gray to pale gray, gravely sand (pumaceous)
32-35		Brownish gray to gray gravely sand
35-36		Conglomerate
36-37		Conglomerate, mixed with gneiss grew silty clay (tuff)
37-40		Greenish gray silt clay (tuff) mixed with gravel
40-45		Sandy gravel mixed with gray silty clay
45-46		Conglomerate
46-55		Sandy silt with few gravels

APPENDIX 3 - WELL LOG OF SP 25

Project:	*EAGLE*	**Drilling method:**	*Air Rotary/DTH*
Client:	*Leicester University*	**Rig type:**	*TH 60*
Location:	*Doni B*	**Coordinate: N**	*943140.5*
Shot hole designation:	*SP 25*	**: E**	*568062.56 | 37N*
Shot hole No.:	*SH 2*	**Altitude:**	*1236*
Casing depth (m):	*34.00*	**Inclination:**	*Vertical*
Casing Diameter:	*8.5"*	**SWL:**	*11.00 m*

Well lithologic log

Depth (m)	**Section**	**Lithologic description**
0-10		Pale yellow to reddish brown silty clay
10-12.		Reddish brown silt and sandy clay
12-22.		Sub angular gravel mixed with clayey sand
22-28		Olive gray silty clay
28-30		Fine to medium grained sand mixed with gravel
30-32		Dark gray, slightly weathered vesicular basalt
32-40		Dark gray, fine grained basalt
40-49		Gray, medium grained basalt, locally vesicular
49-51		Pale yellow welded tuff
51-54		
54-70		Dark gray, medium grained basalt

APPENDIX 3 -WELL LOG OF SP 16

Project:	*EAGLE*		**Drilling method:**	*Air Rotary/DTH*
Client:	*Leicester University*		**Rig type:**	*TH 60*
Location:	*Kula*		**Coordinate: N**	886436.8
Shot hole designation:	*SP 16*		**: E**	575890.59 | 37N
Shot hole No.:	*SH 1*		**Altitude:**	2497.6
Casing depth (m):	*8.00*		**Inclination:**	*Vertical*
Casing Diameter:	*10.5"*		**SWL:**	*33.4 m*

Well lithologic log

Depth (m)	Section	Lithologic description
0-1		Grayish clay
1-3.		Gray sandy and silty clay with few gravel
3-5.		Grayish sandy silt with sub rounded gravel
5-10.		Brownish gray, fine grained, moderately to highly weathered basalt.
10-18.		Brownish gray to fine grained slightly weathered basalt
18-35		Dark gray, fine grained basalt
35-44		Same as 18-35, mixed with reddish & yellow clay
44-50		Yellowish gray, moderately weathered scoracious basalt

APPENDIX 3 - WELL LOG OF SP 17A

Project:	*EAGLE*		Drilling method:	*Air Rotary/DTH*
Client:	*Leicester University*		Rig type:	*TH 60*
Location:	*Bele*		Coordinate: N	*854243*
Shot hole designation:	*SP 17 A*		: E	*613879.67 | 37N*
Shot hole No.:	*SH 1*		Altitude:	*2417.6*
Casing depth (m):	*8.00*		Inclination:	*Vertical*
Casing Diameter:	*10.5"*		SWL:	*40.45 m*

Well lithologic log

Depth (m)	Section	Lithologic description
0-1		Dark gray clay
1-2.		Dark gray clay mixed with olive gray silty clay
2-4.		Olive gray silty clay with few gravel
4-7.		Reddish brown, highly weathered scoracious basalt
7-10.		Gray, slightly to moderately weathered scoracious basalt
10-11.		Dark gray, fine grained basalt interbeded with gray scoracious basalt
11-36.		Dark gray, fine grained basalt
36-37		Dark gray, fine grained basalt, intercalated with brownish gray vesicular basalt
37-40		Brownish gray, slightly to moderately weathered vesicular basalt
40-45		Brownish gray, slightly to moderately weathered vesicular basalt, intercalated with fine grained, dark gray basalt
45-50		Brown to dark gray, slightly to moderately weathered scoracious basalt

APPENDIX 3 - WELL LOG OF SP 17B

Project:	*EAGLE*		**Drilling method:**	*Air Rotary/DTH*
Client:	*Leicester University*		**Rig type:**	*TH 60*
Location:	*Bele*		**Coordinate: N**	7°72"83.7'
Shot hole designation:	*SP 17 B*		**: E**	40°03"23.8'
Shot hole No.:	*SH 2*		**Altitude:**	*???*
Casing depth (m):	*8.00*		**Inclination:**	*Vertical*
Casing Diameter:	*10.5"*		**SWL:**	*39.60 m*

Well lithologic log

Depth (m)	Section	Lithologic description
0-2		Dark gray sandy clay
2-3.		Olive gray silty clay with few gravel
3-4.		Moderately weathered fine grained basalt intercalated with silty clay
4-5.		Brown to gray, fine grained, moderately weathered, slightly vesicular basalt
5-8.		Dark gray, fine grained, slightly to moderately weathered basalt
8-29.		Dark gray, fine grained basalt
29-31		Dark gray to brown, fine grained, slightly weathered, locally vesicular basalt
31-36		Gray to brownish gray, slightly to moderately weathered scoracious basalt.
36-43		Dark gray, fine grained, slightly weathered basalt.
43-44		Dark gray basalt intercalated with pale yellow silty clay (Tuff).
44-45		Pale yellow, silty clay (Tuff)
45-48		Moderately weathered scoracious basalt intercalated with silty clay (Tuff)
48-50		Brown to gray, moderately weathered scoracious basalt.

APPENDIX 3 - WELL LOG OF SP 18A

Project:	*EAGLE*		**Drilling method:**	*Air Rotary/DTH*
Client:	*Leicester University*		**Rig type:**	*TH 60*
Location:	*Delo Sebro*		**Coordinate: N**	799874.1
Shot hole designation:	*SP 18 A*		**: E**	667362.99 | 37N
Shot hole No.:	*SH 1*		**Altitude:**	2159.2
Casing depth (m):	*11.50*		**Inclination:**	*Vertical*
Casing Diameter:	*10.5"*		**SWL:**	*47.02 m*

Well lithologic log

Depth (m)	Section	Lithologic description
0-1		Dark to dark brown clay
1-2.		Dark silty clay
2-3.		Dark sandy clay
3-4.		Dark gray clay with very few sand
4-5.		Pale yellow silty clay (tuff) mixed with sand
5-11.		Pale yellow silty clay (Tuff)
11-12.		Dark gray slightly to moderately weathered basalt
12-20.		Dark gray, fine grained basalt
20-24		Gray, fine grained basalt
24-30		Dark gray, fine grained basalt
30-31		Brown, moderately weathered, slightly vesicular basalt, intercalated with reddish brittle baked clay
31-33		Brown, fine to medium grained, moderately weathered, slightly vesicular basalt
33-41		Brown, fine to medium grained, moderately weathered basalt
41-50		Dark gray, slightly weathered fine grained basalt.

APPENDIX 3 - WELL LOG OF SP 18B

Project:	*EAGLE*		Drilling method:	*Air Rotary/DTH*
Client:	*Leicester University*		Rig type:	*TH 60*
Location:	*Delo Sebro*		Coordinate: N	799777.6
Shot hole designation:	*SP 18 B*		: E	667248.67 | 37N
Shot hole No.:	*SH 2*		Altitude:	2156.6
Casing depth (m):	*8.90*		Inclination:	*Vertical*
Casing Diameter:	*10.5"*		SWL:	*47.02 m*

Well lithologic log

Depth (m)	Section	Lithologic description
0-2		Dark gray clay
2-3.		Pale gray to yellowish gray, silty clay with few rounded gravel (Tuff)
3-7.		Pale gray to yellowish gray, silty clay
7-8.		Pale gray silty clay with few rounded gravel.
8-17.		Gray, fine grained, moderately weathered basalt
17-22.		Olive gray, fine grained, moderately weathered basalt
22-23		Olive gray to dark gray, fine grained, slightly to moderately weathered basalt.
23-27		Dark gray, fine grained basalt
27-30		Olive gray to gray, fine grained, slightly weathered basalt
30-31		Olive gray, fine grained, slightly to moderately weathered basalt intercalated with reddish clay
31-34		Brownish, fine grained, moderately weathered vesicular basalt.
34-38		Brownish, fine grained, slightly weathered and slightly vesicular basalt.
38-41		Brownish, fine grained, moderately weathered, vesicular basalt.
41-46		Sandy gravel
46-50		Angular to sub rounded gravel

Trace	1st Arrival from SP 14	Offset from SP 14	1st Arrival from SP 25	Offset from SP 25	1st Arrival from SP 15	Offset from SP 15	1st Arrival from SP 16	Offset from SP 16	1st Arrival from SP 17	Offset from SP 17	1st Arrival from SP 18	Offset from SP 18
72		73.472	0.86	3.642				53.973		-98.663		
73	1.61	74.307	1.19	6.736	0.79	4.53	0.77	53.075	1.26	-97.774		
74	1.68	75.27	1.26	7.231	1.05	5.525	0.4	52.073	1.18	-96.763		
75	1.53	76.106	1.28	7.701	1.07	6.673		51.227	1.36	-95.897		
76	1.47	77.025	1.36	8.258	1.23	7.292	0.88	50.319	1.44	-94.953		
77	1.37	78.811	1.44	9.208				-48.746	1.32	-93.19	1.417	-168.296
78		79.863	1.49	9.785			0.45	-47.89		-92.177	1.092	-167.256
79		80.968	1.53	10.664				-46.854		-91.058	1.178	-166.14
80	1.32	82.048	1.57	11.922			0.7	-45.57	1.25	-89.866	1.634	-165.007
81	1.865	83.049	1.62	12.487			0.78	-44.864	1.47	-88.934	1.359	-164.031
82		85.075	1.73	13.925				-43.345		-87.011		-162.039
83		85.999	1.69	14.868				-42.409		-86.044		-161.092
84	1.8	86.958	1.73	15.551			0.77	-41.777	1.45	-85.159	0.549	-160.159
85	1.6	89.161	1.7	17.249			0.6	-40.362		-83.13		-158.019
86		90.07		17.791				-40.13		-82.418		-157.192

Trace	1st Arrival from SP 14	Offset from SP 14	1st Arrival from SP 25	Offset from SP 25	1st Arrival from SP 15	Offset from SP 15	1st Arrival from SP 16	Offset from SP 16	1st Arrival from SP 17	Offset from SP 17	1st Arrival from SP 18	Offset from SP 18
87		90.536		18.533				-39.251		-81.775	1.005	-156.644
88		92.223	1.63	20.7			0.66	-36.968	1.31	-79.799		-154.831
89		93.016	1.54	21.775			0.66	-35.823	1.33	-78.862		-153.983
90		94.019		22.837				-34.808		-77.811		-152.962
91	1.6	94.695	1.57	24.406			0.76	-32.967	1.42	-76.818	0.6	-152.213
92		94.887	1.62	25.039			0.74	-32.263	1.56	-76.517		-152.014
93	1.72	95.175	1.54	25.893			0.77	-31.376	1.64	-76.124		-151.741
94		97.549	1.58	27.726			0.87	-29.644	1.38	-73.8		-149.357
95		98.189	1.55	27.975				-29.543	1.45	-73.234		-148.711
96		99.279		29.026				-28.578		-72.135		-147.621
97	1.14	101.145	1.44	30.883			0.76	-26.871	1.41	-70.241	0.781	-145.759
98		101.994	1.41	31.865			0.84	-25.889	1.42	-69.349		-144.917
99	1.32	103.773	1.4	33.66			0.91	-24.256		-67.542		-143.147
100	1.236	104.366	1.37	34.523			0.96	-23.28	1.22	-66.895		-142.581
101	1.22	104.879	1.39	35.366			0.94	-22.297	1.33	-66.338	1.034	-142.113
102		106.962		37.408				-20.469		-64.246		-140.053

Trace	1st Arrival from SP 14	Offset from SP 14	1st Arrival from SP 25	Offset from SP 25	1st Arrival from SP 15	Offset from SP 15	1st Arrival from SP 16	Offset from SP 16	1st Arrival from SP 17	Offset from SP 17	1st Arrival from SP 18	Offset from SP 18
103	1.47	107.985	1.31	38.428			0.91	-19.567	1.08	-63.218	2.19	-139.045
104	1.29	108.982	1.28	39.411			0.91	-18.723	1.05	-62.218	0.933	-138.061
105	0.93	109.955	1.23	40.358			0.9	-17.943	1.09	-61.242	0.802	-137.098
106	1.12	110.915	1.2	41.547			0.87	-16.692	1.23	-60.276		-136.203
108	1.12	111.681	1.15	43.022			0.83	-14.756	1.1	-59.566		-135.646
109	1.24	112.684	1.14	43.995			0.8	-13.922	1.15	-58.571		-134.664
110		113.681		44.966				-13.112		-57.584		-133.69
111		114.862		46.599				-11.267		-56.525		-132.715
112		114.505		46.719			0.69	-10.793		-57.016	1.287	-133.251
113		115.475		47.965				-9.481	1.28	-56.185		-132.451
114	1.39	117.198	1.1	50.236			0.5	-7.086	1.26	-54.808		-131.103
115	0.7	118.093	1.03	51.274			0.46	-6.038	1.29	-54.052		-130.347
116	1.07	118.783	1.04	52.194			0.41	-5.085	1.23	-53.552	0.756	-129.839
117		119.861	1.03	53.301			0.33	-3.997	1.25	-52.584		-128.862
118	0.93	121.531	0.92	55.043			0.08	-2.322	1.12	-51.117	0.92	-127.371
119	0.91	122.198	0.97	55.951			0.07	-1.336	1.42	-50.702		-126.923
120	0.86	123.015	0.94	56.925			-0.02	-0.344	1.37	-50.106	0.73	-126.29
121		124.384	0.88	58.634			0.08	1.464	1.3	-49.216	0.76	-125.306
122		125.181		59.522			0.14	2.328		-48.621	0.77	-124.663

Trace	1st Arrival from SP 14	Offset from SP 14	1st Arrival from SP 25	Offset from SP 25	1st Arrival from SP 15	Offset from SP 15	1st Arrival from SP 16	Offset from SP 16	1st Arrival from SP 17	Offset from SP 17	1st Arrival from SP 18	Offset from SP 18
123		126.227	1.35	60.682			0.2	3.475	1.12	-47.852	0.72	-123.822
124		127.197		61.69			0.23	4.457	1.11	-47.086		-122.996
125	1.24	127.819	1.33	61.874			0.23	4.642	1.11	-46.091	0.71	-122.075
126		128.304		62.053				4.993	1.11	-45.356		-121.387
127	1.29	128.761	1.47	62.179			0.33	5.442	1.11	-44.622	0.75	-120.706
128	1.21	129.762	1.41	62.95			0.38	6.486	1.11	-43.514	0.75	-119.609
129	1.22	132.239		65.133			0.58	9.001	1.06	-41.039	0.8	-117.105
130	1.41	133.357	1.58	66.224			0.64	10.096	1.025	-40.036	0.73	-116.061
131	1.36	134.244		67.053			0.67	10.982	1.08	-39.201	0.74	-115.2
132	1.34	136.074	1.32	68.755			0.76	12.814	1.08	-37.468	0.67	-113.414
133		137.222		69.814			0.83	13.967		-36.37		-112.283
134	1.29	138.219	1.37	70.708			0.87	14.977	0.96	-35.383	0.56	-111.275
135		139.243	1.29	71.601			0.89	16.026	0.98	-34.332	0.65	-110.213
136	1.24	141.202	1.38	73.356			0.91	18.021	0.95	-32.371	0.68	-108.214
137	1.22	142.216	1.38	74.321			0.93	19.031	0.93	-31.44	0.62	-107.234
138		143.136		75.13				19.976		-30.495		-106.277
139	1.08	144.991	1.34	76.832			1.01	21.855	0.95	-28.689	0.659	-104.409

Trace	1st Arrival from SP 14	Offset from SP 14	1st Arrival from SP 25	Offset from SP 25	1st Arrival from SP 15	Offset from SP 15	1st Arrival from SP 16	Offset from SP 16	1st Arrival from SP 17	Offset from SP 17	1st Arrival from SP 18	Offset from SP 18
140	1.06	145.907	1.33	77.608			1.02	22.816	0.97	-27.688	0.66	-103.416
141	1.07	146.767	1.34	78.331			1.05	23.725	0.96	-26.734	0.74	-102.475
142	1.05	148.663	1.39	80.011			1.06	25.689	0.99	-24.764	0.7	-100.485
143		149.525		80.746				26.605		-23.81	0.68	-99.545
144	0.94	151.621	1.28	82.573			1.12	28.816	0.97	-21.543	0.7	-97.293
145	1.05	152.554		83.389			1.19	29.804	0.93	-20.531	0.68	-96.289
146	1.12	153.655	1.3	84.412			1.23	30.927	0.91	-19.448	0.74	-95.168
147	1.05	155.826	1.28	86.546			1.21	33.054	0.88	-17.584	0.75	-93.089
148	1.15	157.62	1.31	88.084			1.16	34.99	0.8	-15.534	0.67	-91.102
149	1.2	159.109	1.31	89.383			1.17	36.593	0.79	-13.864	0.7	-89.471
150		159.889		90.015				37.484		-12.857		-88.557
151		161.229	1.36	91.055				39.083	0.74	-11.014		-86.94
152	0.95	162.177	1.33	91.885				40.126	0.68	-9.924	0.98	-85.9
153	0.96	163.19	1.34	92.844			1.17	41.159	0.54	-8.926	0.64	-84.866
154	0.9	164.203	1.28	93.811			1.09	42.182	0.42	-7.957	0.58	-83.842
155	0.9	166.299	1.28	95.8				44.319	0.42	-5.96	0.51	-81.705
156	0.77	167.858	1.28	97.275			1.09	45.918	0.36	-4.524	0.58	-80.107
157	0.86	170.513	1.31	99.691				48.772	0.23	-1.967	0.55	-77.268
158	0.67	170.993	1.32	99.95				49.545	-0.01	-0.521	0.59	-76.565

APPENDIX 5- FIRST ARRIVAL DATA AS OBTAINED IN THE RAW FORMAT

(Eg taken from SP 16)

Trace No.	First arrival	?
79.991	0.693	1
80.982	0.699	1
84.027	0.693	1
84.973	0.483	1
87.929	0.631	1
88.973	0.642	1
90.938	0.676	1
92.035	0.733	1
92.973	0.710	1
94.035	0.733	1
97.009	0.693	1
97.982	0.744	1
98.973	0.841	1
100.982	0.807	1
102.965	0.841	1
103.991	0.807	1
104.965	0.818	1
105.973	0.778	1
107.973	0.750	1
109.000	0.693	1
111.991	0.557	1
114.062	0.403	1
114.956	0.409	1
115.965	0.318	1

APPENDIX 6 – ACTUAL X-T DATA THAT WAS INVERTED TO GIVE THE GEOSEISMIC MODEL

	Info									
Total Points	**Station**	**Altitude**	**Offset**	**t 14**	**t 25**	**t 16**	**t 17**	**t 18**	**t 15**	**Trace #**
1	1250	1300	73.472		1.467					72
2	1251	1312	74.307	13.9945	2.312667	9.61583	17.55567		1.545	73
3	1253	1339	75.270	14.225	2.465167	9.07883	17.30717		1.970833	74
4	1254	1361	76.106	14.214333	2.5635		17.34283		2.191667	75
5	1255	1380	77.025	14.3075	2.736333	9.26650	17.26550			76
6	1256	1637	78.811	14.505167	2.974667		16.85167	29.46634		77
7	1257	1752	79.863		3.120833			28.968		78
8	1259	1868	80.968		3.307333			28.868		79
9	1260	1938	82.048	14.994667	3.557	8.295	16.22767	29.13517		80
10	1261	1976	83.049	15.7065	3.701167	8.257333	16.29233	28.6975		81
11	1263	2110	85.075		4.050833					82
12	1264	2093	85.999		4.168					83
13	1265	2109	86.958	16.293	4.321833	7.732833	15.64317	27.24217		84
14	1267	2291	89.161	16.460167	4.574833	7.327				85
15	1268	2451	90.07							86
16	1269	2529	90.536					27.11234		87
17	1271	2570	92.223		5.08	6.821333	14.60983			88
18	1272	2579	93.016		5.169167	6.6305	14.47367			89
19	1273	2576	94.019			5.801333				90
20	1275	2609	94.695	17.3825	5.637667		14.223			91
21	1276	2633	94.887		5.793167	6.117167	14.31283			92
22	1277	2613	95.175	17.5825	5.8555	5.999333	14.32733			93
23	1279	2653	97.549		6.201	5.810667	13.68			94
24	1280	2693	98.189		6.2125		13.65567			95
	Info									

Total Points	Station	Altitude	Offset	t 14	t 25	t 16	t 17	t 18	t 15	Trace #
25	1282	2704	99.279							96
26	1283	2686	101.145	17.9975	6.587167	5.2385	13.11683	25.07417		97
28	1286	2682	103.773	18.6155		4.952667				99
29	1287	2672	104.366	18.630333	7.123833		12.36917			100
30	1288	2663	104.879	18.699833	7.284333	4.656167	12.38633	24.7195		101
31	1289	2659	106.96201							102
32	1291	2666	107.98501	19.467502	7.714667	4.171167	11.61633	25.36417		103
33	1292	2655	108.98201	19.453668	7.8485	4.0305	11.41967	23.94317		104
34	1293	2637	109.95501	19.255835	7.956333	3.8905	11.297	23.65167		105
35	1294	2635	110.91501	19.605835	8.1245	3.652	11.276			106
36	1295	2626	111.37901		8.2405		9.9705			107
37	1297	2587	111.68101	19.733502	8.320333	3.289333	11.02767			108
38	1298	2622	112.68401	20.020668	8.4725	3.120333	10.91183			109
39	1300	2605	113.68101							110
40	1302	2595	114.86201							111
41	1303	2588	114.50501			2.488833		23.4955		112
42	1304	2570	115.47501				10.64417			113
43	1305	2568	117.19801	20.923002	9.472667	1.681	10.39467			114
44	1307	2542	118.09301	20.382168	9.575667	1.466333	10.29867			115
45	1308	2531	118.78301	20.867168	9.739	1.2575	10.15533	22.39584		116
46	1309	2506	119.86101		9.9135	0.996167	10.014			117
47	1311	2507	121.53101	21.185168	10.09383	0.467	9.6395	22.1485		118
48	1312	2503	122.19801	21.276335	10.29517	0.292667	9.870333			119
49	1313	2491	123.01501	21.362502	10.4275	0.037333	9.721	21.77834		120
50	1314	2476	124.38401		10.65233	0.324	9.502667	21.64434		121

	Info									
Total Points	Station	Altitude	Offset	t 14	t 25	t 16	t 17	t 18	t 15	Trace #
51	1316	2477	125.18101			0.528		21.54717		122
52	1317	2483	126.22701		11.46367	0.779167	9.095333	21.357		123
53	1318	2488	127.19701			0.972833	8.957667			124
54	1323	2463	127.81901	22.543168	11.64233	1.003667	8.791833	21.05584		125
56	1326	2486	128.76101	22.750168	11.83317	1.237	8.547	20.86767		127
57	1327	2470	129.76201	22.837002	11.90167	1.461	8.362333	20.68484		128
58	1328	2469	132.23901	23.259835		2.080167	7.899833	20.3175		129
59	1330	2450	133.35701	23.636168	12.61733	2.322667	7.697667	20.0735		130
60	1331	2436	134.24401	23.734002		2.500333	7.6135	19.94		131
61	1332	2441	136.07401	24.019002	12.77917	2.895667	7.324667	19.57234		132
62	1334	2496	137.22201							133
63	1335	2499	138.21901	24.326502	13.15467	3.366167	6.857167	19.10584		134
64	1336	2493	139.24301		13.2235	3.561	6.702	19.01884		135
65	1338	2480	141.20201	24.773668	13.606	3.9135	6.345167	18.71567		136
66	1339	2476	142.21601	24.922668	13.76683	4.101833	6.17	18.49234		137
67	1341	2492	143.13601							138
68	1342	2466	144.99101	25.245168	14.14533		5.7315	18.0605		139
69	1343	2461	145.90701	25.377835	14.26467	4.822667	5.584667	17.896		140
70	1345	2478	146.76701	25.531168	14.39517	5.004167	5.415667	17.81917		141
71	1347	2480	148.66301	25.827168	14.72517	5.3415	5.117333	17.4475		142
72	1349	2481	149.52501					17.27083		143
73	1350	2476	151.62101	26.210168	15.04217	5.922667	4.5605	16.9155		144
74	1352	2457	152.55401	26.475668			4.351833	16.72817		145
75	1353	2464	153.65501	26.729168	15.36867			16.60133		146
76	1354	2446	155.82601	27.021002	15.70433	6.719	3.810667	16.26483		147
	Info									

Total Points	Station	Altitude	Offset	t 14	t 25	t 16	t 17	t 18	t 15	Trace #
77	1355	2435	157.62001	27.420002	15.99067	6.991667	3.389	15.85367		148
78	1357	2443	159.10901	27.718168	16.20717	7.268833	3.100667	15.61183		149
79	1358	2443	159.88901				2.142833			150
80	1361	2470	161.22901		16.53583		2.575667			151
81	1362	2442	162.17701	27.979502	16.64417		2.334	15.29667		152
82	1363	2427	163.19001	28.158335	16.814		2.027667	14.78433		153
84	1365	2468	166.29901	28.616502	17.24667		1.413333	14.1275		155
85	1367	2484	167.85801	28.746335	17.4925	8.743	1.114	13.93117		156
86	1368	2476	170.51301	29.278835	17.92517		0.557833	13.428		157
87	1369	2479	170.99301	29.168835			0.076833	13.35083		158

APPENDIX 7: RANGE OF P-WAVE VELOCITIES

ROCK TYPE	**V_P (m/s)**
UNCONSOLIDATED SEDIMENTS	
CLAY	1000 – 2500
SAND, DRY	200 – 1000
SAND, SATURATED	1500 - 2000
SEDIMENTARY ROCKS	
ANHYDRITE	6000
CHALK	2100 – 4500
COAL	1700 – 4500
DOLOMITE	4000 – 7000
LIMESTONE	3900 – 6200
SHALE	2000 – 5500
SALT	4600
SANDSTONE	2000 – 5000
IGNEAOUS AND METAMORPHIC ROCKS	
BASALT	5300 – 6500
GRANITE	4700 – 6000
GABBRO	6500 – 7000
SLATE	3500 – 4400
ULTRAMAFIC ROCKS	7500 – 8500
OTHER	
AIR	300
NATURAL GAS	430
ICE	3400
WATER	1400 – 1500
OIL	1300 - 1400

Declaration

I, the undersigned, herby declare that this thesis is my original work carried out under the supervision of Dr. Tilahun Mammo, has not been presented as a thesis for a degree program in any other university and that all sources of materials used for the thesis are duly acknowledged.

Name Tesfaye Hailu

Signature ____________

Date July 16, 2004

This thesis has been submitted for examination with my approval as university advisor.

Name Dr. Tilahun Mammo

Signature Tilahun Mammo

Date 15.07.04